Steady-State Simulation of Microwave Photonic Systems

by

Amir Ardavan Amini, B.Sc

A thesis submitted to the Faculty of Graduate and Postdoctoral Affairs
in partial fulfilment of the requirements for the degree of

Master of Applied Science
in
Electrical and Computer Engineering

Ottawa-Carleton Institute for Electrical and Computer Engineering
Department of Electronics
Faculty of Engineering
Carleton University
Ottawa, Ontario, Canada

Abstract

The past decade has seen intense activity in the field of microwave photonics in which optical components are used to generate, distribute, control and process microwave and millimeter-wave signals. In parallel there have been significant advances in the area of silicon photonics enabling the inclusion of microwave photonic components into photonic integrated circuits (PICs) ushering in the active area of integrated microwave photonics (IMWP). This has led to the co-existence of electrical and optical components at the level of the integrated circuit. The existence of electrical and optical devices at the same design level requires design tools that can handle components belonging to both physical domains simultaneously for performing system simulation. The technique presented in this thesis addresses this need by presenting a method to perform steady-state simulation of optical-electrical systems using Harmonic Balance (HB). One of the unique features of this method is that it includes phase of the optical signal in finding the steady-state solution of the system. The inclusion of phase in a framework using HB poses several challenges since all system variables in HB are assumed to be periodic and the phase of optical signals is in general non-periodic owing to the non-zero chirp present in laser diodes that are used as drivers for optical systems. Several examples are presented that demonstrate the feasibility of the proposed method and where possible the results are compared with existing techniques.

To my family

Acknowledgments

I would like to express my gratitude to Prof. Pavan Gunupudi, my supervisor, for his guidance and support throughout M.A.Sc. program. I am very grateful for his patience and persuasion during my studies. His constant belief in me has been one of the major motivations to complete this research work and finish my M.A.Sc. program.

It gives me great pleasure to acknowledge the support and advice of Prof. Michel Nakhla over the course of this research. I also gained an excellent insight into the CAD from attending his lectures.

My thanks to all the former and current members of the CAD Research Laboratory in Carleton University for their help and friendship. I am also grateful towards the staff of the Department of Electronics in Carleton University for for being very accommodating and resourceful.

My thank to all my fiernds for the happy moments we shared during the two years of my graduate studies in Ottawa. I would like to make a special mention of my dear friend, Reza, for his help and comments on initial version of this thesis.

Most of all, I would like to express my appreciation to my family for their overwhelming love and kindness during the past twenty-six years. I owe my deepest gratitude to my late grandfather, Mohammad. His memory will be always with me.

Table of Contents

List of Tables

List of Figures

List of Acronyms

Acronyms	Definition
AP	Almost Periodic
APFT	Almost Periodic Fourier Transform
BE	Backward Euler
BJT	Bipolar Junction Transistor
BVP	Boundary-Value-Problem
CAD	Computer Aided Design
CAL	Computer Aided Learning
DFT	Discret Fourier Transform
FDM	Finite Differences Method
FMT	Frequency Mapping Technique
G-DFT	Generalized Discret Fourier Transform
HAM	Homotopy Analysis Methods
HB	Harmonic Balance

IMDD	Intensity Modulated Direct Detection
IMWP	Integrated Microwave Photonic
IVP	Initial-Value-Problem
KCL	Kirchhoffs Current Law
LD	Laser Diode
LPF	Low Pass Filter
MATLAB	Matrix Laboratory Software
MDFT	Multi-Dimensional Fourier Transform
MNA	Modified Nodal Analysis
MOSFET	Metal-Oxid-Semiconductor Field-Effect Transistor
MRHB	Multi-Rate Harmonic Balance
NR	Newton-Raphson
OPALS	Optoelectronic, Photonic, and Advanced Laser Simulator
OptiSPICE	Opto-Electronic Circuit Design Software
PIC	Photonic Integrated Circuit
PD	Photo Diode
QR	Quasi Periodic
RF	Radio Frequency
RoF	Radio over Fiber

SM	Shooting Method
SOAs	Semiconductor Optical Amplifier
SPICE	Simulation Program with Integrated Circuit Emphasis
TAHB	Transient Assistant Harmonic Balance
TLLM	Transmission Line Laser Modeling
TLM	Transmission Line Modeling
TR	Trapezoidal Rule
VCVS	Voltage Controlled Voltage Source
WDM	Wavelength Division Multiplexing

List of Symbols

Symbols	Definition
α	Linewidth enhancement factor.
α_d	HAM damping factor.
α_i's	Thermal coefficients.
β	Spontaneous emission coefficient.
ϵ	Gain comparison factor.
$\varphi(t)$	Optical phase.
$\frac{d\varphi}{dt}$	Optical chirp.
γ	Mode confinement factor.
γ_0	Differential quantum efficiency.
Γ	DFT matrix.
$\mathbf{\Gamma_G}$	G-DFT.
λ_i	i_{th} truncated frequency.
λ_m	Basis frequency of FMT.

Λ	HB frequency truncation.
ω	System frequency of excitation.
ω_c	Optical carrier frequency.
$\boldsymbol{\rho}$	Permutation matrix.
$\boldsymbol{\psi}$	Right hand side of NR iterations.
τ_d	Time delay.
τ_n	Carrier lifetime.
τ_p	Photon lifetime.
a_k^N	k_{th} Fourier coefficient of laser diode carrier density.
$\boldsymbol{b(t)}$	Independent source vector of MNA formulation.
$\bar{\boldsymbol{B}}$	Independent source vector of HB formulation.
c	Speed of light in free space.
$\mathbf{C}$	Memory matrix of MNA formulation.
$E_i(t)$	Imaginary part of optical signal.
$E_r(t)$	Real part of optical signal.
$\boldsymbol{f(x(t))}$	Non-linear vector of MNA formulation.
$\boldsymbol{F(\bar{X})}$	Non-linear vector of HB formulation.
g_0	Gain slope constant.
$\mathbf{G}$	Conductance matrix of MNA formulation.

h	Step size of integration technique .
h_p	Plancks constant.
$I_D(t)$	Electrical current .
$\mathbf{J}$	Jacobian matrix in NR iterations.
K	New tone introduced in the proposed method due to the effect of optical phase.
M	Number of trunctated frequencies.
$N(t)$	Carrier density of laser diode.
N_t	Carrier density at transparency.
$S(t)$	Photon density of laser diode.
T	Time period of a periodic waveform.
T_{global}	Global time period of an AP waveform.
$\bar{\boldsymbol{t}}_{\boldsymbol{s}}$	Vector of sampling time-points.
$p(t)$	Electrical power.
V_L	Active layer volume parameter.
$\bar{\boldsymbol{X}}$	Solution vector of HB formulation.
$\boldsymbol{X}_s$	Vector of response samples in the time-domain.
$\boldsymbol{x(t)}$	Vector of system variables.
$\mathbf{Y}$	HB conductance matrix.

Chapter 1

Introduction

1.1 Background and Motivation

Recent years have witnessed a growing interest in the field of microwave photonics, an interdisciplinary area studying the interaction between optical and microwave/mm-wave signals, for a wide variety of applications such as low-noise and high-frequency microwave sources, high-dynamic-range microwave photonic analog links, true-time-delay phased array antennas, frequency-tunable high-Q microwave filters and high-speed analog to digital converters [1–5]. These applications have been introduced for the generation, distribution, processing and control of microwave and millimeter-wave signals through photonic systems. Research activity over the past few years [5–9] has also shown interest in bringing microwave photonics to the silicon chip in order to replace parts of electrical circuitry that presents challenges such as signal-degradation, high pin-out densities and limited bandwidth.

With the imminent presence of electrical and microwave photonic components in the same level of design hierarchy, the need for an efficient design tool that handles such multi-disciplinary systems is paramount. Several methods [10–22] have been reported for simulation of systems that include both electrical and optical components.

Typically these methods do not include the optical phase in their analysis without which prediction of interference effects of optical signals cannot be performed. Recently, a SPICE-like time-domain optoelectronic simulator, OptiSPICE, [23] was introduced that uses both magnitude and phase of the complex envelope of optical signals in its formulation to ensure the capture of interference effects; moreover OptiSPICE uses a Modified Nodal Analysis (MNA) formulation [24] for including both optical and electrical elements in the same system of equations ensuring a self-consistent solution of the optoelectronic system. In this method, the optoelectronic system is modeled using a set of differential non-linear equations which can be solved in time domain using integration techniques [24, 25].

In several situations a steady-state simulation is adequate to analyze system performance as is the case with typical circuits encountered in microwave photonics. Generally finding the steady-state results using a transient simulation is time-consuming as the system needs to be simulated until the transients die down.

Several methods can be found in literature [26–36] in order to obtain the steady-state solution of non-linear electrical circuits. Of these methods Harmonic Balance (HB) [26–29] is widely applied for simulation of analog radio frequency (RF) and microwave systems. In this approach, the steady state response of an electrical system with respect to periodic excitations is approximated using truncated Fourier series in order to form a set of nonlinear algebraic equations which typically is solved using Newton's method. There have been attempts in order to use HB for laser diodes [37, 38] and optoelectronic systems [39]; however these methods do not consider phase of the optical signals during their analysis.

1.2 Contributions

In this thesis a technique is proposed to perform steady-state simulation of microwave photonic circuits consisting of optical and electrical components using Harmonic Balance considering the effect of optical phase on optical signals. The inclusion of optical phase in HB analysis raises several issues since optical phase is a non-periodic signal and HB assumes all system variables to be periodic.

The theory developed in this thesis highlights the problem of handling phase of optical signals in HB simulation and presents a solution to overcome the issue. The specific contributions of the thesis are as follows:

- In chapter 4, the effect of the non-periodic optical phase generated in laser diodes is investigated and modeled into the HB simulation framework.
- A model for an optical fiber operating in linear regime is developed to be used in conjunction with the HB framework.

1.3 Organization of the Thesis

This thesis consists of six chapters. The current chapter presents the motivations for this work and outlines the organization of the thesis. Chapter 2 provides a review of conventional transient and steady-state electrical circuit simulation. This chapter starts with a brief review of MNA formulation as applied to electrical and optical-electrical systems and is followed by a review on current steady-state simulation techniques with more emphasizes on HB simulation and its traditional implementation difficulties. Practical solutions provided in literature to issues encountered in the HB simulation are also presented. This is followed by a history of existing optoelectronic system and circuit simulators. Of these approaches the OptiSPICE framework is chosen as the basis for our proposed steady-state optoelectronic simulation method.

Chapter 3 gives a background of optical signal infrastructure used in the development of OptiSPICE and includes a review of the OptiSPICE modeling approach for inclusion of optical signals in an MNA-type formulation. Some of the optical device models such as laser diode, multi-mode fiber, and interference based devices developed in OptiSPICE are also described.

Chapter 4 provides a detailed explanation of the issues arising from the phase of optical signal especially in the case of the laser diode and develops the theory to overcome these problems. Detailed models of laser diode and optical fiber that can be used in the HB framework are also presented. In order to verify the accuracy of the proposed method, in Chapter 5, three numerical examples are presented ranging from a Radio-over-Fiber (RoF) link to a system that applies heterodyning to generate a microwave signal which uses a feedback circuit to correct the drift in the output of the laser diode. Lastly, conclusions and future work are presented in Chapter 6.

Chapter 2

Overview of Circuit Simulation Techniques

Before introducing the proposed technique, it is necessary to review basic concepts and previous approaches used to simulate optoelectronic circuits and systems. This chapter is organized as follows: the first section provides a brief overview of a transient SPICE-like simulation framework which today is the most prevalent technique used for simulation of nonlinear electrical circuits; it is followed with a section providing an overview of Harmonic Balance simulation technique which to the date is the method of choice for simulation of nonlinear analog RF and microwave systems. The last section presents a brief review of previous attempts to simulate optoelectronic circuits and systems.

2.1 Basics of Circuit Simulation

Most commercial transient simulators typically have use a SPICE-like approach to formulate the electrical circuit into system equations. In this approach, the system equations for a general electrical circuit are formulated using Modified Nodal Analysis (MNA) [24] in the following form:

$$\mathbf{G}\boldsymbol{x}(\boldsymbol{t}) + \mathbf{C}\frac{\mathbf{d}\boldsymbol{x}(\boldsymbol{t})}{\mathbf{dt}} + \boldsymbol{f}(\boldsymbol{x}(\boldsymbol{t})) = \boldsymbol{b}(\boldsymbol{t}), \tag{2.1}$$

where $\mathbf{G} \in \mathbb{R}^{n\times n}$ is the conductance matrix, $\mathbf{C} \in \mathbb{R}^{n\times n}$ represents the energy storage in elements, n is the number of system variables, the vector $\boldsymbol{f}(\boldsymbol{x}(t)) \in \mathbb{R}^n$ captures the nonlinear nature of the devices, $\boldsymbol{b}(t) \in \mathbb{R}^n$ is the time-dependent forcing vector, and the vector $\boldsymbol{x}(\boldsymbol{t}) \in \mathbb{R}^n$ consists of node voltages, device currents, and stored charges of nonlinear capacitive elements. Typically, this system of equations is solved by discretization of $\boldsymbol{x}(\boldsymbol{t})$ into several time steps using numerical integration techniques [25] such that the nonlinear set of differential equations in (2.1) is converted to a nonlinear algebraic set of equations as:

$$\mathbf{A}\boldsymbol{x}(\boldsymbol{t}) + \boldsymbol{f}(\boldsymbol{x}(\boldsymbol{t})) = \boldsymbol{b}(\boldsymbol{t}). \tag{2.2}$$

The equation above can be solved using numerical integration techniques. For instance, using the Backward Euler (BE) method [25], the response at $t = t_i + h$ is found by using the derivative only at the current time point as:

$$\boldsymbol{x}(\boldsymbol{t_i} + \boldsymbol{h}) = \boldsymbol{x}(\boldsymbol{t_i}) + h\dot{\boldsymbol{x}}(\boldsymbol{t_i} + \boldsymbol{h}), \tag{2.3}$$

resulting in the set of difference equations:

$$(\mathbf{G} + \frac{\mathbf{C}}{\mathbf{h}})\boldsymbol{x}(\boldsymbol{t_i} + \boldsymbol{h}) + \boldsymbol{f}(\boldsymbol{x}(\boldsymbol{t_i} + \boldsymbol{h})) = \frac{\mathbf{C}}{\mathbf{h}}\boldsymbol{x}(\boldsymbol{t_i}) + \boldsymbol{b}(\boldsymbol{t_i}), \tag{2.4}$$

where h is the integration time step and can be customized based on transition speed of the response. Practically the time step (h) can be decreased if the response is undergoing sharp edges and increased if the response is more steady.

On the other hand, in Trapezoidal Rule (TR) [25] the solution vector at $t = t_i + h$ is found by using the derivative at both current and previous time steps as:

$$\boldsymbol{x}(\boldsymbol{t_i} + \boldsymbol{h}) = \boldsymbol{x}(\boldsymbol{t_i}) + \frac{h}{2}(\dot{\boldsymbol{x}}(\boldsymbol{t_i} + \boldsymbol{h}) + \dot{\boldsymbol{x}}(\boldsymbol{t_i})), \tag{2.5}$$

leading to the following set of difference equations:

$$(\mathbf{G}+\frac{\mathbf{2C}}{\mathbf{h}})\boldsymbol{x}(\boldsymbol{t_i} + \boldsymbol{h})+\boldsymbol{f}(\boldsymbol{x}(\boldsymbol{t_i} + \boldsymbol{h})) = (\frac{\mathbf{2C}}{\mathbf{h}}-\mathbf{G})\boldsymbol{x}(\boldsymbol{t_i})+\boldsymbol{b}(\boldsymbol{t_i})+\boldsymbol{b}(\boldsymbol{t_i} + \boldsymbol{h})-\boldsymbol{f}(\boldsymbol{x}(\boldsymbol{t_i})). \tag{2.6}$$

Typically, the nonlinear algebraic equations in (2.2) are solved using Newton-Raphson (NR) iterations [25]. These iterations are performed by repeatedly solving the following equation:

$$\mathbf{J}\boldsymbol{\Delta x^j} = \boldsymbol{\psi}, \tag{2.7}$$

where,

$$\boldsymbol{\psi} = \mathbf{A}\boldsymbol{x}^j + \boldsymbol{f}(\boldsymbol{x}^j) - \boldsymbol{b}, \tag{2.8}$$

$$\mathbf{J} = \mathbf{A} + \frac{\mathbf{d}\boldsymbol{f}(\boldsymbol{x}^j)}{\mathbf{dt}}, \tag{2.9}$$

$$\boldsymbol{\Delta x^i} = \boldsymbol{x}^j - \boldsymbol{x}^{j-1}. \tag{2.10}$$

The transient results typically provide a good understanding of the behavior of

the system; however, in several application areas such as telecommunication and microwave design obtaining the steady-state solution of system is generally adequate to study the system performance. For many lightly damped systems, conventional transient simulation takes many periods of excitation in order to reach the steady state solution which is typically computationally expensive and usually takes a long amount of time.

To overcome the difficulty with conventional transient simulation, a variety of methods have been proposed to find the steady-state solution more efficiently. The next section provides a review of traditional steady-state simulation techniques and in particular Harmonic Balance (HB) simulation which today is the most used simulation technique for finding the steady-state solution of analog RF and microwave systems.

2.2 Steady State Simulation

Several steady-state simulation techniques [26–36] have been derived to obtain the steady-state response of electrical circuits and systems. In general, the system solution at steady state with respect to a periodic excitation is found by satisfying the two-point constraint as

$$\boldsymbol{x}(\boldsymbol{T}) = \boldsymbol{x}(\mathbf{0}). \tag{2.11}$$

In Finite Differences Method (FDM) [26], a finite difference approximation is used in order to discretize the system into a finite set of time points resulting in a system of nonlinear algebraic equations which is solved in the time-domain using Newton's method.

In Shooting Method (SM) simulation [26, 28, 30], the steady-state solution of the system is found purely in the time-domain by treating the problem as a Boundary-Value-Problem (BVP). SM can be viewed as a transient simulation which accelerates

the finding of the steady state solution by adjusting the initial condition of each one-period transient simulation. In this method, $\boldsymbol{x(t)}$ is discretized in the time interval $[0 \;\; T]$ using integration techniques where the solution is found by solving:

$$\boldsymbol{\psi(x(0), 0, T) - x(0)} = 0, \tag{2.12}$$

in which $\boldsymbol{\psi}$ is the state transition and $\boldsymbol{\psi(x(0), 0, T) = x(T)}$. The nonlinear algebraic system equations in (2.12) are typically solved using Newton methods which refer to the Shooting-Newton algorithms [26]. Non-uniform time points selection algorithms can be used in order to increase the efficiency of time-domain techniques for solving highly non-linear systems [26].

On the other hand, in Harmonic Balance (HB) [26–29] the response of the system at steady-state is found in frequency-domain using truncated Fourier series expansion. Generally time-domain methods are superior for solving single tone systems having several spikes and sharp response edges, demanding use of a large number of harmonics to capture the steady-state waveforms, which in turn considerably increases HB simulation time and memory usage [40]. Generally most of the optoelectronic and microwave photonic systems are multi-tone systems having Almost-Periodic (AP) responses at steady-state. Traditionally, finding the steady-state solution of systems under multi-tone excitation using a time-domain method, is not efficient since finding the common period of the system is computationally a burden [40].

Harmonic Balance can be seen as a variation of early Galerkin methods which approximate the solution of differential equations by unknown coefficients. The term "*Harmonic Balance*" was originated since the method was initially developed for non-linear electrical circuits [41] by balancing currents between the linear and non-linear sub-networks. The modern form of HB formulation was given by Nakhla and Vlach [29] in 1978 through reducing the system into smaller sub-circuits, either being

nonlinear or linear. The resultant framework was originally called piecewise Harmonic Balance. In some publications, HB is mentioned as a mixed-domain technique because the non-linearities are evaluated in time-domain while the linear sub-circuits are analyzed in the frequency-domain.

The next subsection provides a review of HB simulation framework in its modern form, followed by subsections describing general HB implementation difficulties and practical solutions provided in literature.

2.2.1 Harmonic Balance System Equations

Harmonic Balance [26–29] is one of the several techniques used in finding the steady-state response of the system directly without performing a lengthy transient simulation. In HB, generally the steady-state solution with respect to a periodic excitation over a truncated set of frequencies is written as:

$$\boldsymbol{x(t)} = \bar{\boldsymbol{X}}_{\boldsymbol{o}} + \sum_{\lambda_k \epsilon \Lambda, \lambda_k \neq 0} \bar{\boldsymbol{X}}_{\boldsymbol{k}}^{\boldsymbol{c}} \boldsymbol{cos}(\lambda_k t) + \bar{\boldsymbol{X}}_{\boldsymbol{k}}^{\boldsymbol{s}} sin(\lambda_k t), \tag{2.13}$$

where, Λ is the set of truncated frequencies, and $\bar{\boldsymbol{X}}_{\boldsymbol{o}}$, $\bar{\boldsymbol{X}}_{\boldsymbol{k}}^{\boldsymbol{c}}$, $\bar{\boldsymbol{X}}_{\boldsymbol{k}}^{\boldsymbol{s}}$ are the vectors containing unknown coefficients required to be found in order to obtain the steady-state solution of the system. Following the regular procedure of HB [26, 27], (2.13) is substituted into (2.1) to obtain a set of nonlinear algebraic equations as:

$$\mathbf{Y}\bar{\boldsymbol{X}} + \boldsymbol{F}(\bar{\boldsymbol{X}}) = \bar{\boldsymbol{B}}, \tag{2.14}$$

where, $\mathbf{Y} \in \mathbb{R}^{n(2M+1)\times n(2M+1)}$ is a block diagonal matrix formed using MNA matrices as:

$$\mathbf{Y} = \begin{bmatrix} \mathbf{G} & 0 & 0 & 0 & 0 & 0 & 0 & 0 & 0 \\ 0 & \mathbf{G} & \lambda_1\mathbf{C} & 0 & 0 & 0 & 0 & 0 & 0 \\ 0 & -\lambda_1\mathbf{C} & \mathbf{G} & 0 & 0 & 0 & 0 & 0 & 0 \\ 0 & 0 & 0 & \mathbf{G} & \lambda_2\mathbf{C} & 0 & 0 & 0 & 0 \\ 0 & 0 & 0 & -\lambda_2\mathbf{C} & \mathbf{G} & 0 & 0 & 0 & 0 \\ \vdots & \vdots & 0 & 0 & 0 & \ddots & \ddots & \vdots & 0 \\ \vdots & \vdots & \vdots & \vdots & 0 & \ddots & \ddots & \vdots & 0 \\ \vdots & \vdots & \vdots & \vdots & 0 & 0 & 0 & \mathbf{G} & \lambda_M\mathbf{C} \\ 0 & 0 & 0 & 0 & 0 & 0 & 0 & -\lambda_M\mathbf{C} & \mathbf{G} \end{bmatrix}. \tag{2.15}$$

$\boldsymbol{F}(\bar{\boldsymbol{X}}) \in \mathbb{R}^{n(2M+1)}$ and $\bar{\boldsymbol{B}} \in \mathbb{R}^{n(2M+1)}$ respectively represent non-linearities and independent sources as:

$$\boldsymbol{F}(\bar{\boldsymbol{X}}) = \begin{bmatrix} \boldsymbol{F_0}(\bar{\boldsymbol{X}}) \\ \boldsymbol{F_1^C}(\bar{\boldsymbol{X}}) \\ \boldsymbol{F_1^S}(\bar{\boldsymbol{X}}) \\ \vdots \\ \boldsymbol{F_M^C}(\bar{\boldsymbol{X}}) \\ \boldsymbol{F_M^S}(\bar{\boldsymbol{X}}) \end{bmatrix}, \qquad \bar{\boldsymbol{B}} = \begin{bmatrix} \boldsymbol{B_0} \\ \boldsymbol{B_1^C} \\ \boldsymbol{B_1^S} \\ \vdots \\ \boldsymbol{B_M^C} \\ \boldsymbol{B_M^S} \end{bmatrix}. \tag{2.16}$$

Typically, the nonlinear algebraic equations in (2.14) are solved using NR iterations [26, 27]. These iterations are performed by repeatedly solving:

$$(\mathbf{Y} + \frac{\mathbf{dF}(\bar{\mathbf{X}}^{\mathbf{i}})}{\mathbf{dX}^{\mathbf{i}}})\boldsymbol{\Delta}\bar{\boldsymbol{X}}^{\mathbf{i}} = \mathbf{Y}\bar{\boldsymbol{X}}^{\mathbf{i}} + \boldsymbol{F}(\bar{\boldsymbol{X}}^{\mathbf{i}}) - \bar{\boldsymbol{B}}, \tag{2.17}$$

where,

$$\boldsymbol{X_s} = \boldsymbol{\Gamma}^{\mathbf{-1}}\boldsymbol{\rho}\bar{\boldsymbol{X}}, \tag{2.18}$$

$$\boldsymbol{F}(\bar{\boldsymbol{X}}) = \boldsymbol{\Gamma}\rho^{\mathbf{T}}\boldsymbol{f}(\boldsymbol{X_s}), \tag{2.19}$$

$$\frac{\mathbf{dF}(\bar{\mathbf{X}})}{\mathbf{d}\bar{\mathbf{X}}} = \boldsymbol{\Gamma}\boldsymbol{\rho}^{\mathbf{T}}\frac{\mathbf{df}(\mathbf{X_s})}{\mathbf{dX_s}}\boldsymbol{\rho}\boldsymbol{\Gamma}^{\mathbf{-1}}, \tag{2.20}$$

$\boldsymbol{\Gamma} \in \mathbb{R}^{n(2M+1)\times n(2M+1)}$ is the block diagonal Fourier transform matrix, $\boldsymbol{\rho}$ is the permutation matrix for reordering equations, and $\boldsymbol{X}_s \in \mathbb{R}^{n(2M+1)}$ is the vector of response samples in the time-domain found at sampling time points:

$$\bar{\boldsymbol{t}}_{\boldsymbol{s}} = \begin{bmatrix} t_o & t_1 & \cdots & t_{2M} \end{bmatrix}^T \quad for \quad 0 \leq t_i < T \tag{2.21}$$

where T is the time period system generally related to the smallest frequency component in Λ [26, 27].

Since in HB the response of the system at steady-state is approximated by a truncated Fourier series, first step in finding the generalized Fourier coefficients is to define a set of truncated frequencies constituting all possible system frequency combinations. In defining the truncation scheme, one must consider that the scheme has to efficiently include a large number of distinct frequencies to capture the nonlinearities in the system. In simple words, if too few harmonics are considered, the results are inaccurate; if too many are considered, the approach becomes impractical.

The next subsection provides two of the well-known frequency truncation schemes for handling situations involving AP signals having only two-tones. Generalization of

a two-tone scheme to a multi-tone case is typically a straight forward procedure.

2.2.2 Frequency Truncation Schemes

Box Truncation Scheme

In this approach the frequency truncation is built by defining two constant terms as a limitation for each tone [40, 42]. As a result, frequencies are given by:

$$\lambda_i = |k_1\omega_1 + k_2\omega_2|, \tag{2.22}$$

where,

$$(0 \leqslant k_1 \leqslant K_1, |k_2| \leqslant K_2) \quad and, (k_1 \neq 0 \quad if \quad k_2 < 0), \tag{2.23}$$

form the truncation scheme. Box truncation scheme is widely used for systems having one of the frequency excitations considerably dominant [40]. For such a system, K_i corresponding to the dominant tone is defined reasonably large compared to other tones, which effectively reduces the computation cost of system simulation by minimizing the size of HB system equations without loose of accuracy. For system having two tones, the truncated frequencies are plotted in Figure 1 and listed in Table 1.

Diamond Truncation Scheme

Diamond frequency truncation [40, 42] is constructed by defining a constant term as a limitation for fundamental tones. Hence all the frequencies are given by (2.2.2), in which

$$(0 \leqslant |k_1| + |k_2| \leqslant K_3, 0 \leqslant k_1) \quad and, (0 \leqslant k_2 \quad if \quad k_1 = 0). \tag{2.24}$$

Generally the diamond truncation scheme is preferable for systems having tones with almost equal strength due to a better flexibility of choosing mixing product [40]. Figure 2 presents a schematic of diamond frequency truncation scheme where only

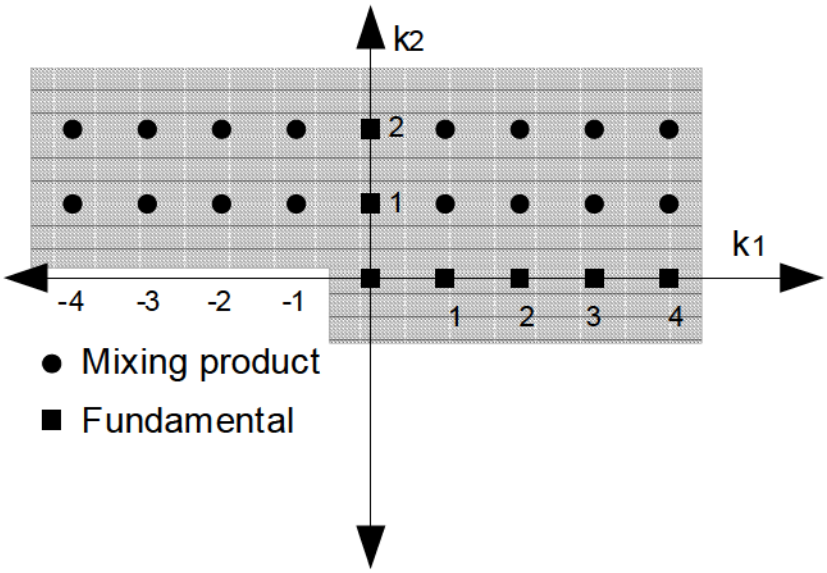

Figure 1: Schematic of box truncation scheme for $K_1 = 4$ and $K_2 = 2$.

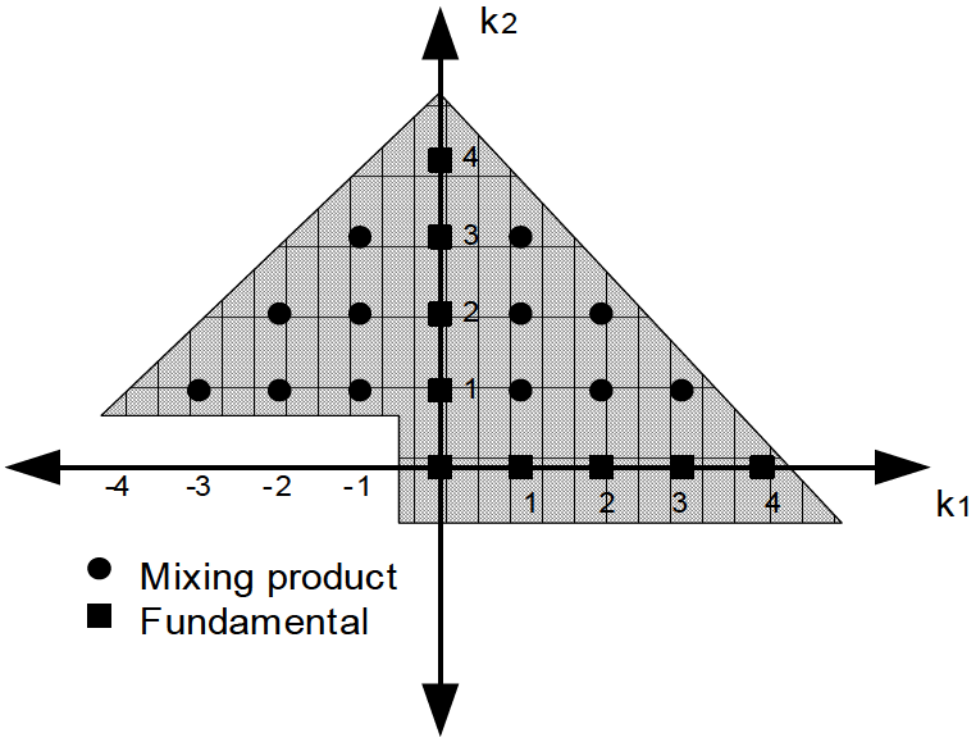

Figure 2: Schematic of diamond truncation scheme for $K_3 = 4$.

two tones are involved. These frequencies are listed in Table 2.

Table 1: Truncated frequencies of box truncation scheme for $K_1 = 4$ and $K_2 = 2$.

k_1	k_2	λ_i	
0	0	0	DC
1	0	ω_1	first order products
0	1	ω_2	
2	0	$2\omega_1$	second order products
0	2	$2\omega_2$	
± 1	1	$\omega_2 \pm \omega_1$	
3	0	$3\omega_1$	third order products
± 1	2	$2\omega_2 \pm \omega_1$	
± 2	1	$\omega_2 \pm 2\omega_1$	
4	0	$4\omega_1$	fourth order products
± 2	2	$2\omega_2 \pm 2\omega_1$	
± 3	1	$\omega_2 \pm 3\omega_1$	
± 3	2	$2\omega_2 \pm 3\omega_1$	fifth order products
± 4	1	$\omega_2 \pm 4\omega_1$	
± 4	2	$2\omega_2 \pm 4\omega_1$	sixth order product

Table 2: Truncated frequencies of diamond truncation scheme for $K_3 = 4$.

k_1	k_2	λ_i	
0	0	0	DC
1	0	ω_1	first order products
0	1	ω_2	
2	0	$2\omega_1$	second order products
0	2	$2\omega_2$	
± 1	1	$\omega_2 \pm \omega_1$	
3	0	$3\omega_1$	third order products
0	3	$3\omega_2$	
± 1	2	$2\omega_2 \pm \omega_1$	
± 2	1	$\omega_2 \pm 2\omega_1$	
4	0	$4\omega_1$	fourth order products
0	4	$4\omega_2$	
± 2	2	$2\omega_2 \pm 2\omega_1$	
± 3	1	$\omega_2 \pm 3\omega_1$	
± 1	3	$3\omega_2 \pm \omega_1$	

2.2.3 Harmonic Balance Implementation Issues

The efficiency of HB simulation is dependent on several implementation parameters. This section provides a review of implementation difficulties which arise in a HB implementation along with practical solutions provided in literature.

Initial Guess

The convergence of NR is not always guaranteed unless it is started reasonably close to the solution. Finding a proper initial point is one of the significant issues in implementing a simulator engine and it becomes even more crucial when solving HB equations. Several techniques [26, 27, 42] can be used to improve the initial guess used for NR iterations. One approach is to use the DC solution of the system as the initial guess [40, 42]. In this approach, the system is solved by a DC solver and the obtained results are properly mapped into the HB initial vector. In some systems having long transients, Transient Assistant Harmonic Balance (TAHB) solver [42] is used which solves the system in time-domain for few time periods and maps the result into the HB initial vector. For circuits that are highly nonlinear and contain sharp-edged waveforms, a transient simulation often provides a good initial guess for the starting point of HB [42]. Generally using results generated by a single tone simulation often provide better convergence rate [42]. In this approach, the nonlinear system under multi-tone excitation is simulated for each tone separately, and results obtained from simulations are incorporated to be used as the initial vector.

Homotopy

The Homotopy Analysis Methods (HAM) also called continuation methods [26, 43] refer to techniques that solve nonlinear differential equations by initially reducing the power of the input signal until convergence is achieved. Using this approach, the HB

system equations (2.14) can be rewritten by separating the input sources vector as two vectors representing the DC and AC sources as:

$$\mathbf{Y}\bar{\boldsymbol{X}} + \boldsymbol{F}(\bar{\boldsymbol{X}}) = \bar{\boldsymbol{B}}_{\boldsymbol{dc}} + \alpha_{\mathbf{d}}\bar{\boldsymbol{B}}_{\boldsymbol{ac}}, \tag{2.25}$$

where α_d is a damping factor between 0 and 1. In this technique, the NR iterations begin by taking $\alpha_d = 0$ while using the trivial DC solution as the initial starting vector. The iterations continue by increasing the α_d to 1, which is the trivial full HB solution.

Multi-tone Systems Convergence

Harmonic Balance was originally used for simulation of single tone systems until 1980s [44]. In order to perform an efficient HB simulation for higher level of excitations several issues need to be addressed.

Generally a direct approach to perform a frequency-time domain transformation for an almost periodic signal is to treat the signal as a periodic signal and define the Generalized Discrete Fourier Transform (G-DFT) matrix as:

$$\boldsymbol{\Gamma}_{\mathbf{G}}^{-\mathbf{1}} = \begin{bmatrix} 1 & \cos(\lambda_1 t_0) & \sin(\lambda_1 t_0) & \cdots & \cos(\lambda_M t_0) & \sin(\lambda_M t_0) \\ 1 & \cos(\lambda_1 t_0) & \sin(\lambda_1 t_1) & \cdots & \cos(\lambda_M t_1) & \sin(\lambda_M t_1) \\ \vdots & \vdots & \ddots & \vdots & \vdots & \vdots \\ 1 & \cos(\lambda_1 t_{2M}) & \sin(\lambda_1 t_{2M}) & \cdots & \cos(\lambda_M t_{2M}) & \sin(\lambda_M t_{2M}) \end{bmatrix}. \tag{2.26}$$

The problem in implementing a multi-tone framework is aliasing error [40]. In harmonic balance simulation, this error is generated due to the truncation of an infinite spectrum with a finite number of frequencies. In order to avoid aliasing error

in HB simulation, the minimum sampling rate of a periodic waveform has to be:

$$H \geqslant \frac{2\lambda_{max}}{\lambda_{min}}, \tag{2.27}$$

where λ_{min} and λ_{max} are the smallest and largest frequency components in the truncation respectively. Satisfying the above condition is impractical where AP waveforms have close base frequencies as it results in large HB system equations.

The other problem arises from the conditioning number of G-DFT [40]. The condition number presents the sensitivity of a function to changes and errors. For a multi-tone waveform if the time point samples are not selected carefully, the transform matrix becomes ill-conditioned which magnifies the numerical and aliasing errors [40]. These facts generally turn a straight forward approach for solving a multi-tone HB system equation inaccurate and practically useless.

Several attempts have been made to facilitate above difficulties in a multi-tone HB framework. Almost Periodic Fourier Transform (APFT) approaches [26, 27, 40, 45–49] were presented by Chua and Uchida [48, 49] where extra time points are used for sampling an AP waveform which in turn makes the DFT matrix tall-rectangular. In this approach, the transpose of the matrix is used to make the matrix inversion possible as:

$$\bar{\boldsymbol{X}} = (((\boldsymbol{\Gamma_G}^{-1})^{\mathbf{T}}(\boldsymbol{\Gamma_G}^{-1}))^{-1}(\boldsymbol{\Gamma_G}^{-1})^{\mathbf{T}}\boldsymbol{X_s}. \tag{2.28}$$

The result found by using the above method is not the exact solution but reasonably close.

Several algorithms [26, 27, 45–47] have been proposed in literature to generate a proper selection of orthogonal sampling vectors for constructing G-DFT. In [46] a randomly oversampling time point selection approach in a period of $3T_{global}$ is used to improve G-DFT conditioning number. The Modified Gram-Schmidt algorithm [46] is then performed in order to select the most orthogonal sampling vectors.

In Multi-Dimensional Fourier Transform (MDFT) [50–52] technique, an auxiliary m-dimensional function in time-domain is replaced by the original single dimensional function to adapt the quasi-periodic waveforms for the MDFT as:

$$\boldsymbol{x^{'}(t_1, t_2, \cdots, t_m)}_{t_1,t_2,\cdots,t_m=t} = \boldsymbol{x(t)}, \tag{2.29}$$

where $x^{'}(t_1, t_2, \cdots, t_m)$ is defined as:

$$\boldsymbol{x^{'}(t_1, t_2, \cdots, t_m)} = \sum_{\sum_{i=1}^{m} k_i\omega_i} \bar{\boldsymbol{X}}_{k_1,k_2,\cdots,k_m} e^{jk_i\omega_i t_i}, \tag{2.30}$$

The high computational cost of multi-dimensional discretization is the main disadvantage of the MDFT technique.

Frequency Mapping Technique (FMT) also called false frequency method [26, 53] is widely used in most available commercial simulators. The basic concept of FMT relies on the fact that non-linear coefficients are independent of truncated frequencies and are only related to system variable coefficients. So an artificial frequency (λ_m) is defined which makes all components in frequency scheme become a unique integer multiple of λ_m. As a result, the multi-tone HB equations system can be treated as a single tone which can be solved using single-dimensional simple DFT. For example, having two base frequencies, the mapped frequency is defined as:

$$\begin{aligned} \omega_1 &\mapsto \lambda_m, \\ \omega_2 &\mapsto (1 + 2K_1)\lambda_m, \end{aligned} \tag{2.31}$$

for the box truncation scheme and as:

$$\begin{aligned} \omega_1 &\mapsto K_3\lambda_m, \\ \omega_2 &\mapsto (K_3 + 1)\lambda_m, \end{aligned} \tag{2.32}$$

Table 3: Frequency mapping of truncated frequencies presented in Section 2.2.2

index	λ_{mi}	λ_i	
		box truncation	diamond truncation
0	0	0	0
1	λ_m	ω_1	$\omega_2 - \omega_1$
2	$2\lambda_m$	$2\omega_1$	$2\omega_2 - 2\omega_1$
3	$3\lambda_m$	$3\omega_1$	$\omega_2 - 2\omega_1$
4	$4\lambda_m$	$4\omega_1$	ω_1
5	$5\lambda_m$	$\omega_2 - 4\omega_1$	ω_2
6	$6\lambda_m$	$\omega_2 - 3\omega_1$	$2\omega_2 - \omega_1$
7	$7\lambda_m$	$\omega_2 - 2\omega_1$	$\omega_2 - 3\omega_1$
8	$8\lambda_m$	$\omega_2 - \omega_1$	$2\omega_1$
9	$9\lambda_m$	ω_2	$\omega_2 + \omega_1$
10	$10\lambda_m$	$\omega_1 + \omega_2$	$2\omega_2$
$\vdots$	$\vdots$	$\vdots$	$\vdots$
14	$14\lambda_m$	$2\omega_2 - 4\omega_1$	$2\omega_2 + \omega_1$
15	$15\lambda_m$	$2\omega_2 - 3\omega_1$	$3\omega_1$
$\vdots$	$\vdots$	$\vdots$	$\vdots$
17	$17\lambda_m$	$2\omega_2 - \omega_1$	$\omega_2 + 3\omega_1$
18	$18\lambda_m$	$2\omega_2$	$2\omega_2 + 2\omega_1$
$\vdots$	$\vdots$	$\vdots$	$\vdots$

for the diamond truncation. The method has been generalized for the box truncation scheme [26, 40] but to date, no explicit scheme had been introduced for the diamond truncation with more than two basis frequencies involved [40]. Table 3 presents the relation between the artificial and original spectra for set of truncated frequencies presented in Section 2.2.2.

Recently, Multi-Rate Harmonic Balance (MRHB) [54] technique is proposed for an efficient frequency selection in simulation framework. MRHB enables the designer to allow different parts of the circuit to have different dominating frequencies, resulting in a more accurate and faster HB simulation.

In case of very large scale integrated circuits, using preconditioned linear solvers [30, 31, 42, 55–59], and in particular Krylov-subspace methods, significantly accelerates HB simulation of medium-nonlinear systems. Using these techniques, the high computation cost and memory usage of conventional HB are avoided by iterative techniques. These techniques which typically approximate the NR iterations are also called inexact-Newton Raphson methods.

2.3 Optoelectronic Simulation

In the past recent, several approaches [10–22] have been reported for simulation of systems that include both electrical and optical components. Chatoyant [10, 11] models nonlinear components around a hierarchically heterogeneous at the system-level called Ptolemy [10, 11, 60] using low frequency piecewise linear models. The defined models construct a linear network to be simulated in the frequency-domain. The optical device models are classified under three different categories as analytical, empirical, and lumped models. For analytical models, devices are modeled directly based on the equations that represent the device physics. The empirical models are developed for devices such as multiple-quantum-well modulators by using measured data. Lumped models such as photodiode and trans-impedance amplifier are derived from the execution of lower-level simulation and analysis tools.

Optoelectronic, Photonic, and Advanced Laser Simulator (OPALS) [12] being a Computer Aided Learning (CAL) software uses Transmission-Line Laser Modeling (TLLM) [13] for modeling laser sources. In this approach the semiconductor laser model has been developed by the addition of a frequency-dependent gain model to the traditional Transmission-Line Modeling (TLM) method.

iSmile and iFrost [14, 15] perform a mixed-mode methodology by modeling some components in the time-domain and other components in the frequency-domain.

Microwave-Harmonica [17] uses two-port network models for a number of optical components which its application is limited for Intensity Modulated Direct-Detection (IMDD) lightwave systems. DEX's SOLUS [18] is based on the SPICE-like circuit simulator with a separate sub-simulator called SONAR for analyzing optical signals in the optical domain. IBM's OLAP [19] is an APL program which combines the higher-level abstraction of communication system simulators such as SYSTID with the low-level detail of optical component simulators. BOSS [20] has a performance that is limited for lightwave systems as it cannot utilize circuit design information in the system analysis, and was originally designed for single wavelength systems. COMSIS [21] based on time-domain techniques, is a simulation package for design of communication systems and includes a limited optical models library. In [22] SPICE is used as a CAD tool for optoelectronic system simulation by implementing equivalent SPICE models for optical devices.

Typically these methods do not include phase of the optical signal in their analysis which without prediction of interference effects of optical signals cannot be performed. Recently, a SPICE-like time-domain optoelectronic simulator, OptiSPICE, [23] was introduced that uses both magnitude and phase of the complex envelope of optical signals in its formulation to ensure the capture of interference effects; moreover, OptiSPICE uses a Modified Nodal Analysis (MNA) [24] formulation for including both optical and electrical elements in the same system of equations ensuring a self-consistent solution of the optoelectronic system. Since optical device models used in the proposed framework are similar to those developed in OptiSPICE, it is necessary to present a brief review of the OptiSPICE simulator framework and its modeling approach for modeling optical signals. The next Chapter provides an overview of OptiSPICE simulation framework followed by several optical component models developed in OptiSPICE.

2.4 Summary

In this chapter a background of conventional electrical circuit simulation techniques was provided. The first section presented the traditional transient simulation approach for simulation of non-linear electrical circuits. Next, an overview of steady-state simulation methods was presented including a detailed description of the HB simulation technique. Several HB implementation difficulties were explained along with practical solutions provided in literature. Finally a brief review of existing optoelectronic circuit simulation methods was presented. Of these approaches the OptiSPICE simulator framework is selected as the basis of our proposed method.

Chapter 3

OptiSPICE Transient Simulator

Electrical circuits are simulated using computer-aided tools by representing them using MNA equations that are formed using Kirchhoff's Current Law (KCL). This type of a formulation is possible since the electric and magnetic fields in typical electrical components are conservative leading to unique voltages and currents. Unlike electrical domain, the electric and magnetic fields in the optical domain are non-conservative [23]; as such, a direct approach using voltages and currents for formulating optical circuits and systems into an MNA formulation is not possible. In order to introduce optical signals into a SPICE-like [61] simulator framework an appropriate representation of the electrical and magnetic field of light has to be used. This chapter describes the basic concepts developed in OptiSPICE [23] in order to formulate an optical signal into an MNA type of formulation. The chapter is organized as follows: the first section provides a general description of an optical signal followed by an overview of the modeling terminology proposed in OptiSPICE to include an optical signal into an MNA formulation. It follows with several optical device model examples developed in OptiSPICE. Lastly, in section 3.3 a simple form of the OptiSPICE simulator framework is implemented in MATLAB and simulation results obtained for a simple optical link are presented in an illustrative example.

3.1 Wavelength, Channel, Mode

The relation between frequency and wavelength in the free space is given by

$$f_c = \frac{c}{\lambda_c}, \tag{3.1}$$

where c is the speed of light in the free space as 3×10^8 m/s, λ_c and f are the wavelength and frequency respectively. The speed of propagation in materials is less than c given by a refractive index as

$$n = \frac{c}{v}, \tag{3.2}$$

where v is the speed which light travels in a transparent material. For example, the refractive index of air is given as 1.0003 and typically around 1.5 for glasses.

Differentiating (3.1) around a center wavelength as λ_c we obtain the relation between frequency spacing and wavelength spacing results as

$$\Delta f_c = \frac{c}{\lambda_c^2} \Delta \lambda_c. \tag{3.3}$$

Unlike electrical signals, within the same optical waveguide optical signals have the ability to carry the information in several independent **channels** referred to different carrier frequencies. For instance, an optical fiber may constitute of two separate channels where one channel is in the 1310 nm band and the other in the 1550 nm band. Such a system is referred to as wavelength division multiplexing (WDM) system [62, 63]. In these systems, multiple optical carriers at different wavelengths are modulated and then transmitted through an optical fiber. These signals are then separated at the detector using demultiplex devices. Such a system allows bidirectional communication while increasing the capacity.

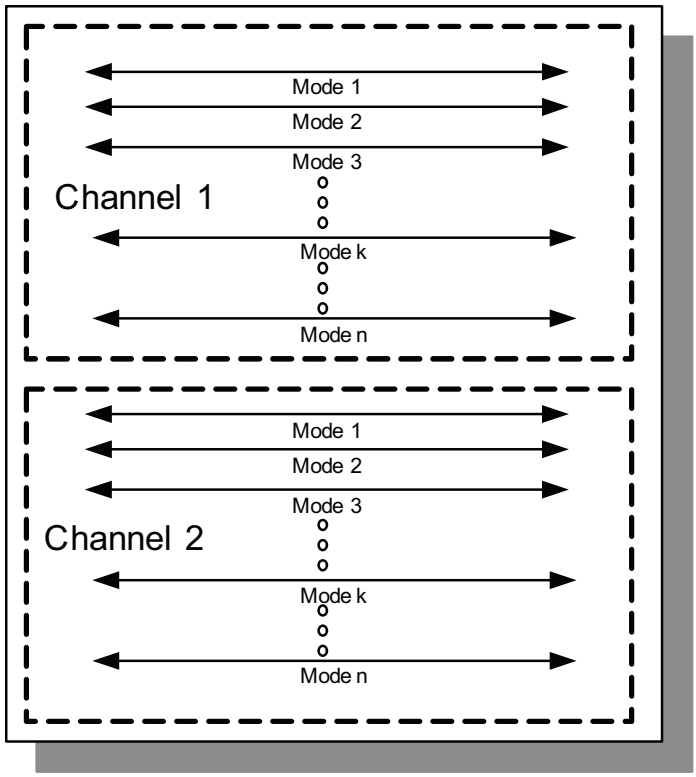

Figure 3: Mode and channel illustration within an optical waveguide.

For most optical components, within each channel the optical energy propagates on an infinite sets of independent electromagnetic **modes** given by the orthogonal solutions of the wave equation; however, generally a finite number of modes are significantly excited. The structure of these modes is dependent on the optical device geometry.

In each particular mode, optical signals propagate in forward and backward direction of propagation. Figure 3 presents a schematic of channel and mode representation for an optical waveguide. As such, the expression for optical energy in a waveguide is written as [23]

$$\mathbb{E}_F(x, y, z, t) = E_F(t) S_i(x, y) e^{i(\omega_c + \varphi_F(t) + nkz_o)} \tag{3.4}$$

$$\mathbb{E}_B(x, y, z, t) = E_B(t) S_i(x, y) e^{i(-\omega_c + \varphi_F(t) + nkz_o)} \tag{3.5}$$

where $S_i(x, y)$ represents the mode shape, $E_F(t)$ and $E_B(t)$ are optical signal envelopes in forward and backward direction of propagations, ω_c is the optical carrier frequency, n is the optical refraction index of k_{th} mode ,and $\varphi_F(t)$ and $\varphi_B(t)$ are the time varying optical phases in forward and backward direction of propagations. Integrating in x and y directions, the resultant optical signal can be represented as [23]

$$E(t, z_o) = E_F(t)e^{i(\omega_c+\varphi_F(t)+nkz_o)} + E_B(t)e^{i(-\omega_c+\varphi_B(t)+nkz_o)}, \tag{3.6}$$

nkz_o can be absorbed into the time varying optical phase as a fixed phase shift resulting in

$$E(t, z_o) = E_F(t)e^{i(\omega_c+\varphi_F(t))} + E_B(t)e^{i(-\omega_c+\varphi_B(t))}. \tag{3.7}$$

For transient simulation, the existence of the carrier frequency which typically is around 100 THz range demands an extremely small step size to be used in the integration technique which in turn considerably increases the simulation time and memory usage. Therefore for transient simulation it is preferable to remove the carrier frequency (ω_c) from (3.7) and represent the signal using its envelope and phase [23].

OptiSPICE proposed a transient self-consistent optoelectronic circuit simulator framework incorporating wavelengths, channels and modes using a traditional MNA formulation through the definition of an *optical node* [23]. Within this framework optical signals are characterized by carrier wavelengths into different optical channels determined by the system topology while each constitutes of a set of optical modes. The mode shapes can be defined using commercial mode solvers or analytical mode shapes such as Bessel functions. For each individual optical mode, two propagating signals are modeled using four state variables. These variables represent magnitude and phase of the complex envelope of the optical signal in forward and backward directions. The advantage of using magnitude and phase representation over real and imaginary parts for complex optical signal in a transient simulator framework will be

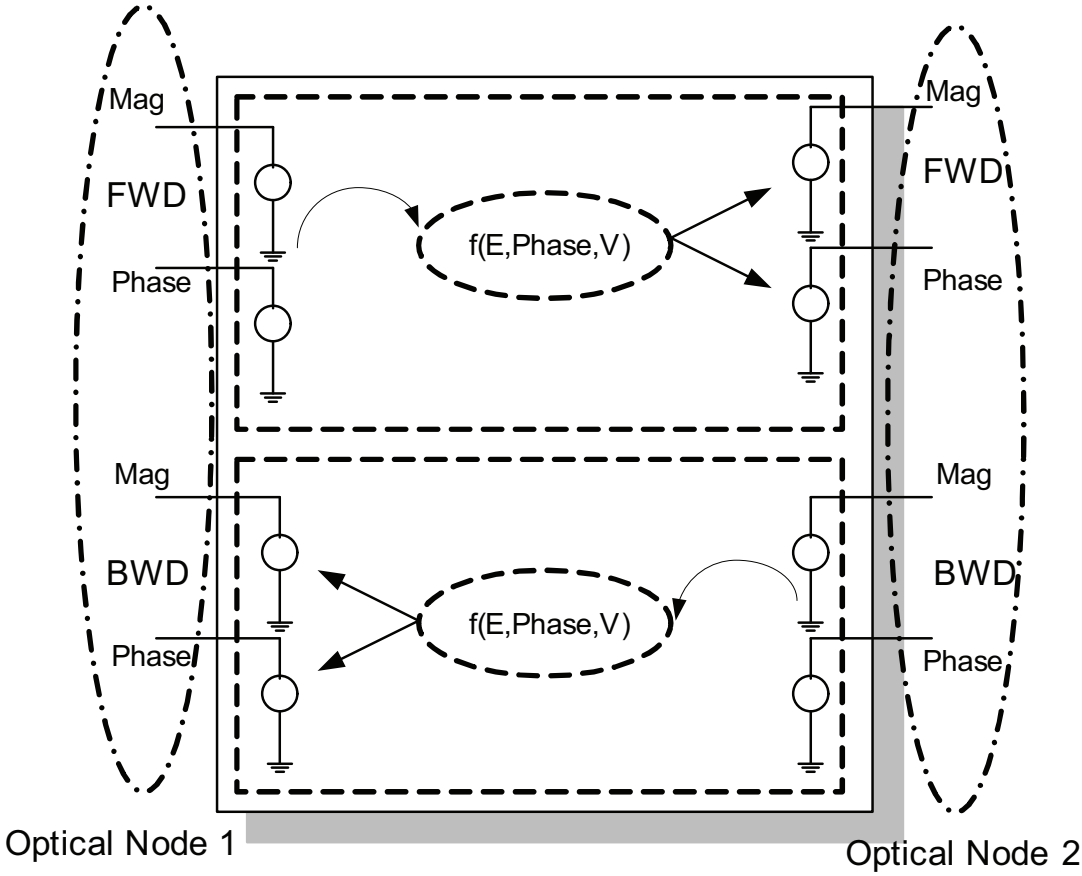

Figure 4: Optical device between two optical nodes.

clarified in the next section where the optical source function is described. Figure 4 represents an illustration of a simple device between two optical nodes for a particular mode developed in OptiSPICE [23].

3.2 Device Modeling

In OptiSPICE [23] optical devices are classified under three main categories based on their operations on the input signals to generate the output signals. *Sources* and *detectors* are modeled either using simple linear elements or complex nonlinear equations. *Direct elements* which take the magnitude and phase of the signal at the input and perform different operations such as attenuation, phase shift, and delay. And

lastly *interference based* elements take the real and imaginary parts of the input and perform several manipulations to produce the output signal. Moreover, OptiSPICE supports a wide variety of electrical SPICE [61] circuit components such as BJTs and MOSFETS. The following subsections provide detailed optical device simulation models developed in OptiSPICE.

3.2.1 Sources and Detectors

Multi-mode Laser Diode

In OptiSPICE the dynamic of the laser diode is modeled by rate equations which describe the relation between carrier density $N(t)$, photon density $S(t)$ and optical phase $\varphi(t)$. As such for a multi-mode temperature dependent laser diode the rate equations are given as [23, 64, 65]

$$\frac{dN(t)}{dt} = \frac{I_D(t) - I_{off}(T)}{qV_L} - \frac{N(t)}{\tau_n} - \sum_{u=1}^{M} g_0(N - N_o)\frac{S_u(t)}{1 + \epsilon S_u(t)} \tag{3.8}$$

$$\frac{dS_u(t)}{dt} = \frac{\gamma\beta_u N(t)}{\tau_n} - \frac{S_u(t)}{\tau_p} + \gamma g_o(N(t) - N_t)(\frac{S_u(t)}{1 + \epsilon S_u(t)}) \tag{3.9}$$

$$\frac{d\varphi(t)}{dt} = \frac{1}{2}\alpha\gamma g_o(N(t) - N_t) - \frac{\alpha}{2\tau_p}, \tag{3.10}$$

$$I_{off}(T) = a_o + a_1 T + a_2 T^2 + \cdots \tag{3.11}$$

where $I_D(t)$ is efficient injected current, $I_{off}(T)$ represents the temperature dependent nature of laser diode [23,65], T is the laser temperature, u subscript presents the mode number, V_L is the active layer volume, q is the electron charge, ϵ is the gain comparison factor, τ_n and τ_p are the carrier and photon lifetime, γ is the mode confinement factor, β is the spontaneous emission coefficient, g_o is the gain slope constant, N_t is the carrier density at transparency for which the net gain is zero, α is the linewidth enhancement factor, and a_is are thermal coefficients determined from parameter extraction.

Then the output power of each mode is determined by [23, 64]

$$p(t) = \frac{V_L \gamma_0 h_p f_c}{2\gamma\tau_p} S(t) \tag{3.12}$$

where γ_0 is the differential quantum efficiency, h_p is Plancks constant and f_c is the optical carrier frequency. The chirp of the laser related to the derivative of the optical phase is given by [64]

$$\Delta f(t) = \frac{1}{2\pi} \frac{d\varphi(t)}{dt}. \tag{3.13}$$

The reason for choosing magnitude and phase variables over real and imaginary parts in OptiSPICE framework is that typical optical sources produce a constant chirp at steady state [23, 64], traditionally in THz range, resulting in oscillation of real and imaginary parts of optical envelope signals at these frequencies which considerably limits the simulation step sizes. Therefore, at steady state, the use of magnitude and phase as state variables addresses the problem of small step sizes during simulation [23].

The above rate equations can be stamped into MNA matrices. This forms the model for the laser diode using rate equations. The output constitutes of optical field envelope and phase. The schematic of laser diode model used in OptiSPICE is presented in Figure 5 [23].

Photodiode

A photodiode is a type of semiconductor which converts the optical signal into an electrical current. In OptiSPICE, the photodiode is implemented using an electrical diode and a photo-current which is determined by the square of electrical field magnitude at its input [23, 66]. Figure 6 presents the schematic of the photodiode model present in OptiSPICE. The output of the filter drives the traditional SPICE diode with extra resistors, capacitor, and inductor at the output.

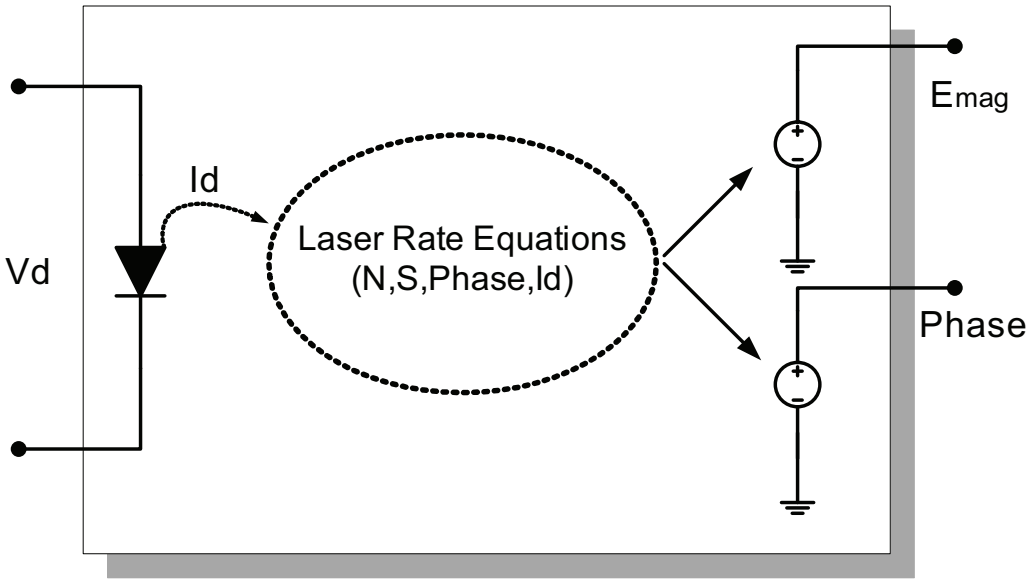

Figure 5: Schematic of single-mode laser diode in OptiSPICE.

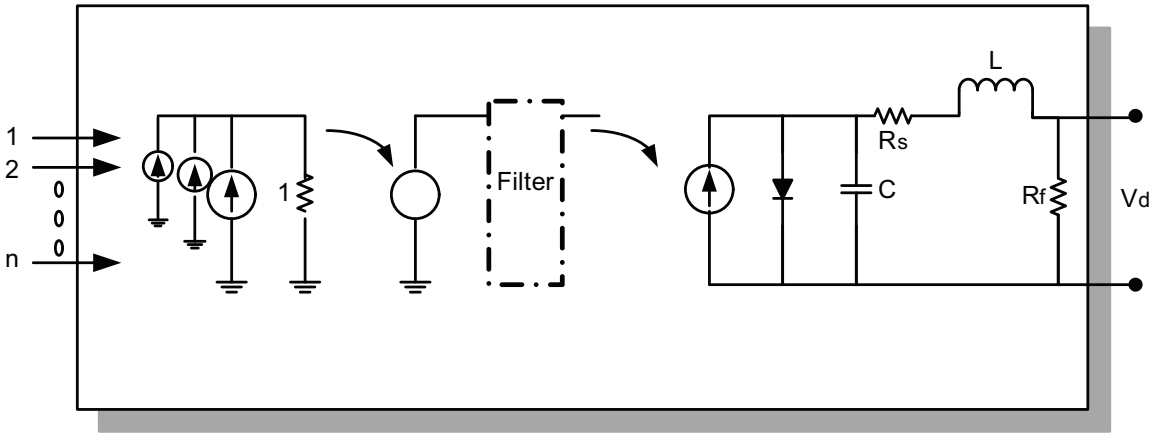

Figure 6: Schematic of photodiode in OptiSPICE.

3.2.2 Direct Elements

Isolator

Most passive optical devices are reciprocal components; as such these devices work exactly the same way if their inputs and outputs are reversed [67]. In many systems it is necessary to have non-reciprocal devices. An example of these devices is the optical isolator. An optical isolator allows an optical signal follows in only one direction and

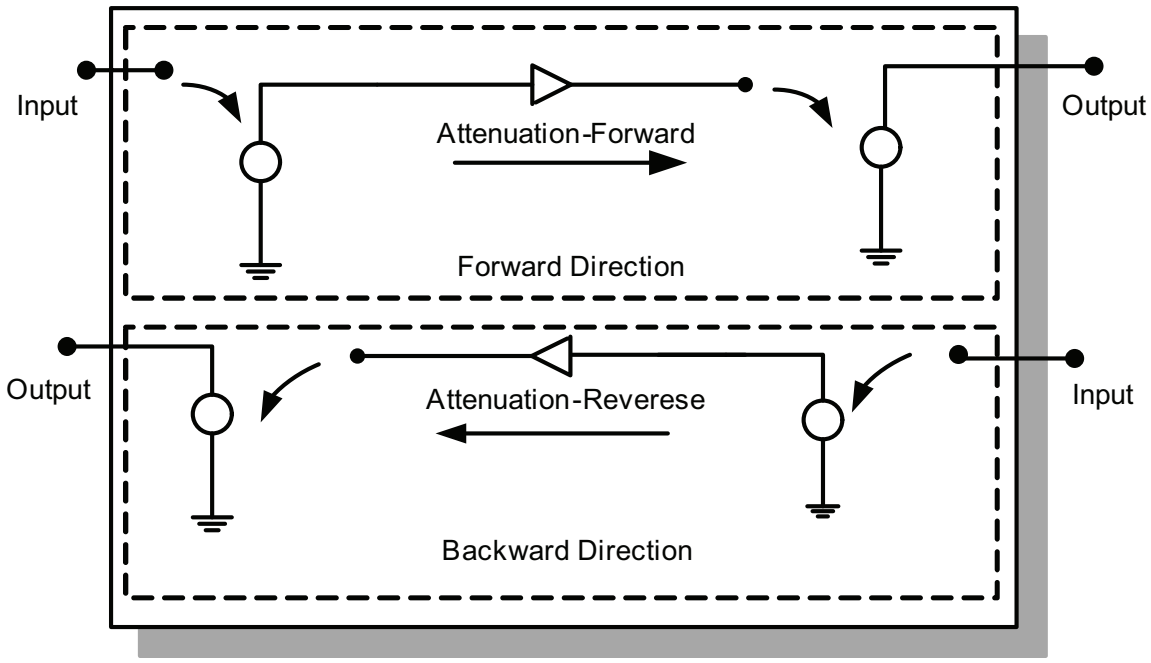

Figure 7: Schematic of a single mode of an isolator in OptiSPICE.

almost blocks signal in the other way. The two important factors of an optical isolator are the insertion loss and isolation. The insertion loss is the loss of the optical signal in forward direction and the isolation is the loss in backward direction which should be as large as possible (in ideal case infinity). In OptiSPICE isolators are modeled using voltage-controlled voltage sources (VCVS). Figure 7 shows an schematic of an isolator presented in OptiSPICE.

Multi-mode Fiber

In OptiSPICE, the multimode fiber is classified as a direct element. The model is implemented such that it takes the magnitude and phase of the optical signal at its input and performs manipulations such as attenuation, phase shift, and delays [23,68, 69] to generate the output. The schematic in Figure 8 presents an illustration of the process involved for a particular mode of the multi mode fiber. As seen the magnitude of each mode is bidirectional, isolated, delayed, and attenuated. The attenuation is

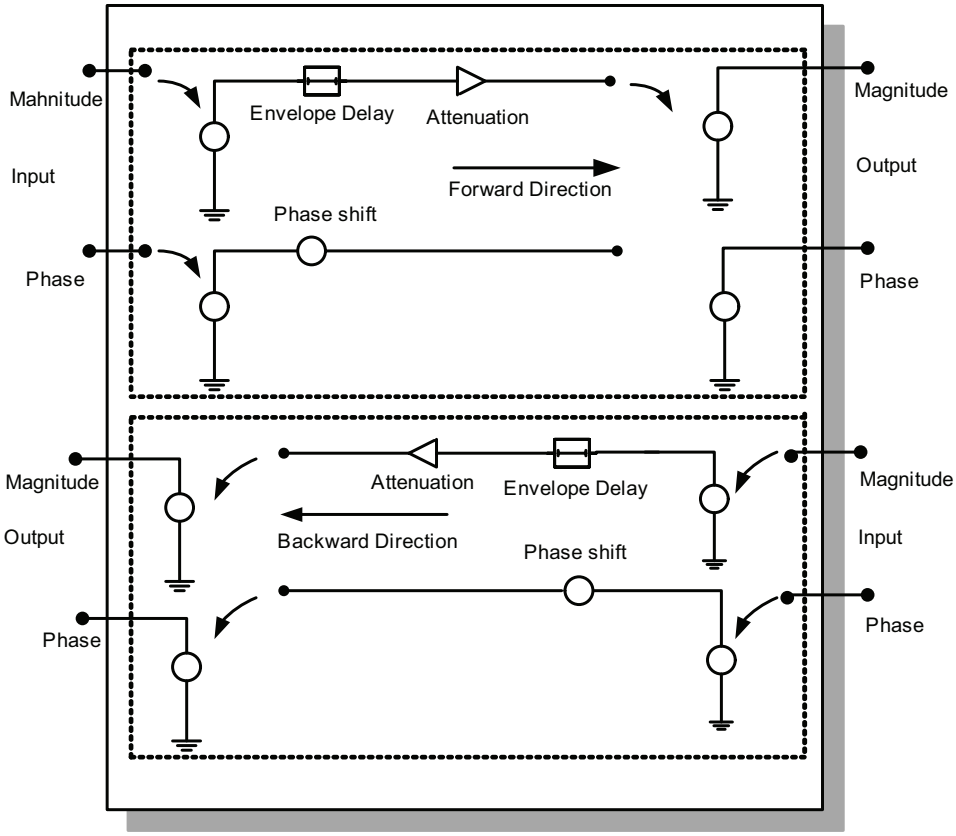

Figure 8: Schematic of a particular mode of a multi-mode fiber in OptiSPICE.

implemented by voltage controlled voltage sources (VCVS). The delay of the envelope which is dependent on the length of the optical fiber and could vary from nanoseconds to seconds is implemented by storing the history of device inputs. The phase shift representing the carrier and phase delay is implemented through a time delay and phase shift between the input and output of the phase input [23, 69].

3.2.3 Interference Based Elements

Generally interference elements refer to optical devices which mix or add different optical signals together. In OptiSPICE interference based elements are modeled using complex interference matrices. The device takes the real (E_r) and imaginary (E_i)

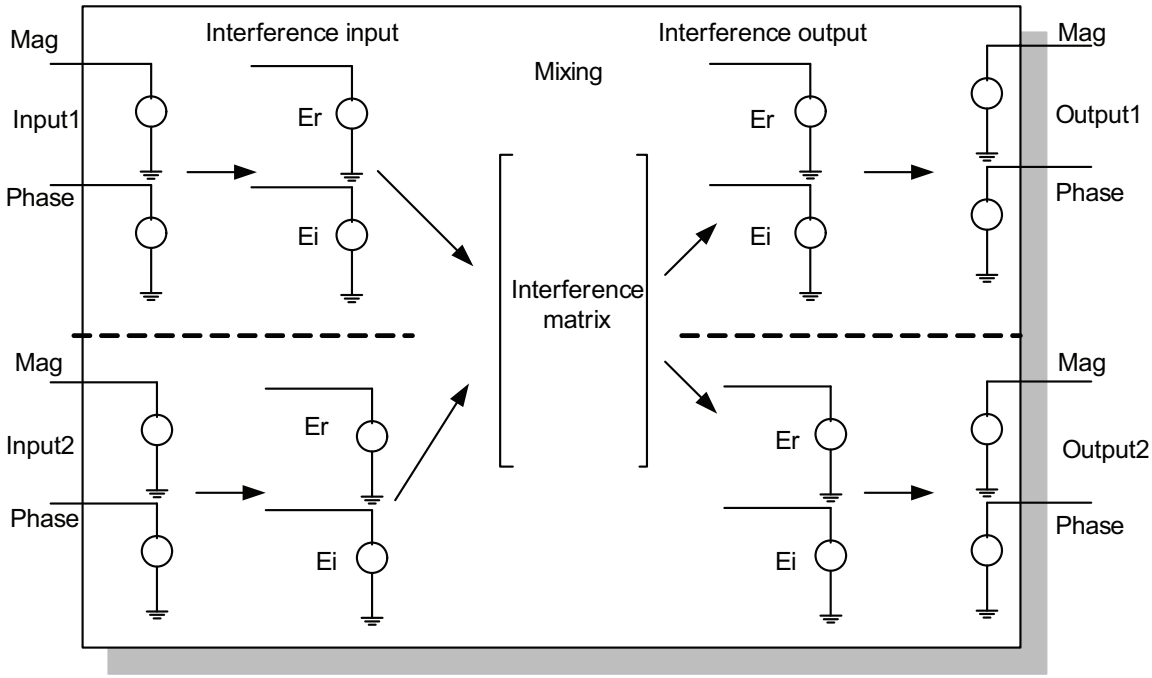

Figure 9: Schematic of a single mode, channel of optical coupler in OptiSPICE.

parts of the optical signal at its input and produces outputs. To illustrate the modeling approach used in OptiSPICE, models of some basic optical interference based components are provided.

For a single mode, single channel 2×2 *optical coupler* the relation between complex input/output is given by a complex interference matrix as

$$\begin{pmatrix} E_{1o} \\ E_{2o} \end{pmatrix} = \begin{pmatrix} k_1 & ik_2 \\ ik_2 & k_1 \end{pmatrix} \begin{pmatrix} E_{1i} \\ E_{2i} \end{pmatrix}, \tag{3.14}$$

where E_{1o}/E_{2o} and E_{1i}/E_{2i} respectively are coupler complex outputs and inputs resulting to real and imaginary parts representation as

$$\begin{pmatrix} E^r_{1o} \\ E^i_{1o} \\ E^r_{2o} \\ E^i_{2o} \end{pmatrix} = \begin{pmatrix} k_1 & 0 & 0 & -k_2 \\ 0 & k_1 & k_2 & 0 \\ 0 & -k_2 & k_1 & 0 \\ k_2 & 0 & 0 & -k_1 \end{pmatrix} \begin{pmatrix} E^r_{1i} \\ E^i_{1i} \\ E^r_{2i} \\ E^i_{2i} \end{pmatrix}, \tag{3.15}$$

where

$$k_1 = \sqrt{1-c}, \tag{3.16}$$

$$k_2 = p\sqrt{c}, \tag{3.17}$$

where p and c are constant coupling factors which are determined based on coupler function. The schematic for a cross coupler described above is shown in Figure 9.

The *beam splitter* splits the optical signal with a ratio dependent on device function at the output. For examples, a 50-50 2×1 beam splitter transmit the signal in forward direction as

$$\begin{pmatrix} E^F_{1o} \\ E^F_{2o} \end{pmatrix} = \frac{1}{\sqrt{2}} \begin{pmatrix} 1 \\ 1 \end{pmatrix} E^F_i, \tag{3.18}$$

and in backward direction as

$$E^B_i = \frac{1}{\sqrt{2}} \begin{pmatrix} 1 & 1 \end{pmatrix} \begin{pmatrix} E^B_{1o} \\ E^B_{2o} \end{pmatrix}. \tag{3.19}$$

The above input/output relations can be stamped into MNA matrices. It is also possible to model more complex devices by mixing different optical components together. The example given in OptiSPICE [23] is an optical circulator which is formed using three optical isolators and three optical splitters.

3.3 Illustrative Example

A simple version of OptiSPICE was implemented in MATLAB for use in this thesis as OptiSPICE is implemented in C and is difficult to extend for the purpose of this thesis. The MATLAB simulator is written such that it takes a SPICE-like netlist to form the optoelectronic MNA formulation. For solving nonlinear differential MNA equations either BE or TR can be used as a choice of integration. At each time step NR iterations are performed in order to solve the nonlinear algebraic equations. Several electrical components along with optical devices described in this chapter are implemented and simulated in the time-domain to illustrate the performance of the framework. The simulation results for a simple optical link obtained from MATLAB simulator are presented in this section as an illustrative example. Results obtained from OptiSPICE are also shown for comparison.

The optical link shown in Figure 10 constitutes of a BJT transistor driving a laser diode which in turn is connected to an optical fiber. The output of the fiber is connected to a photodiode which converts the optical signal into electrical current. The laser input current is a pulse with .5 ns in length and rise and fall times of .1 ns. The simulation result of the laser diode driving current is presented in Figure 11. As seen both simulators predict the same response.

Figure 12 (a) and (b) show the magnitude and phase of the optical signal at the output of the laser diode. The linear increase of the optical phase is due the constant chirp existing in optical sources shown in Figure 15.

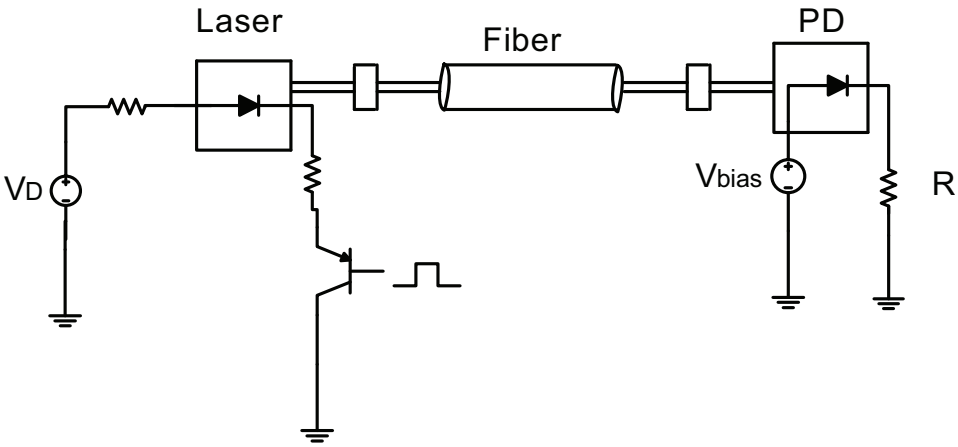

Figure 10: Illustrative example link schematic.

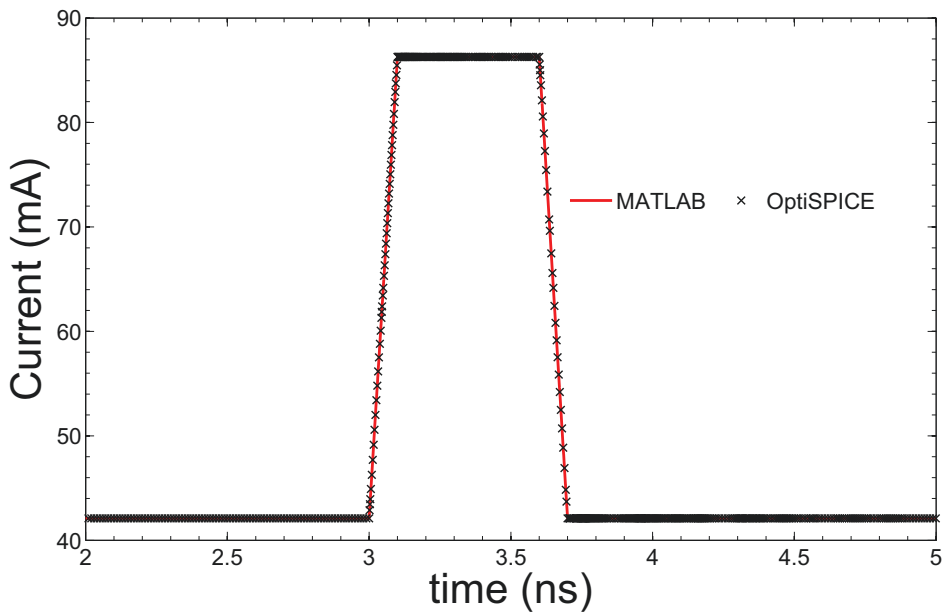

Figure 11: Current of the laser diode.

The output of the laser diode then is passed through an optical fiber which is modeled using delay elements and phase shifters. The optical fiber has a nominal time delay of 5 ns with a signal attenuation of .8. Figure 13 (a) and (b) show the magnitude and phase of the optical signal at the output of the optical fiber. As seen the optical signal is attenuated, delayed and shifted. At the photodiode, this optical signal is converted to an electrical voltage. Figure 14 presents the photodiode current

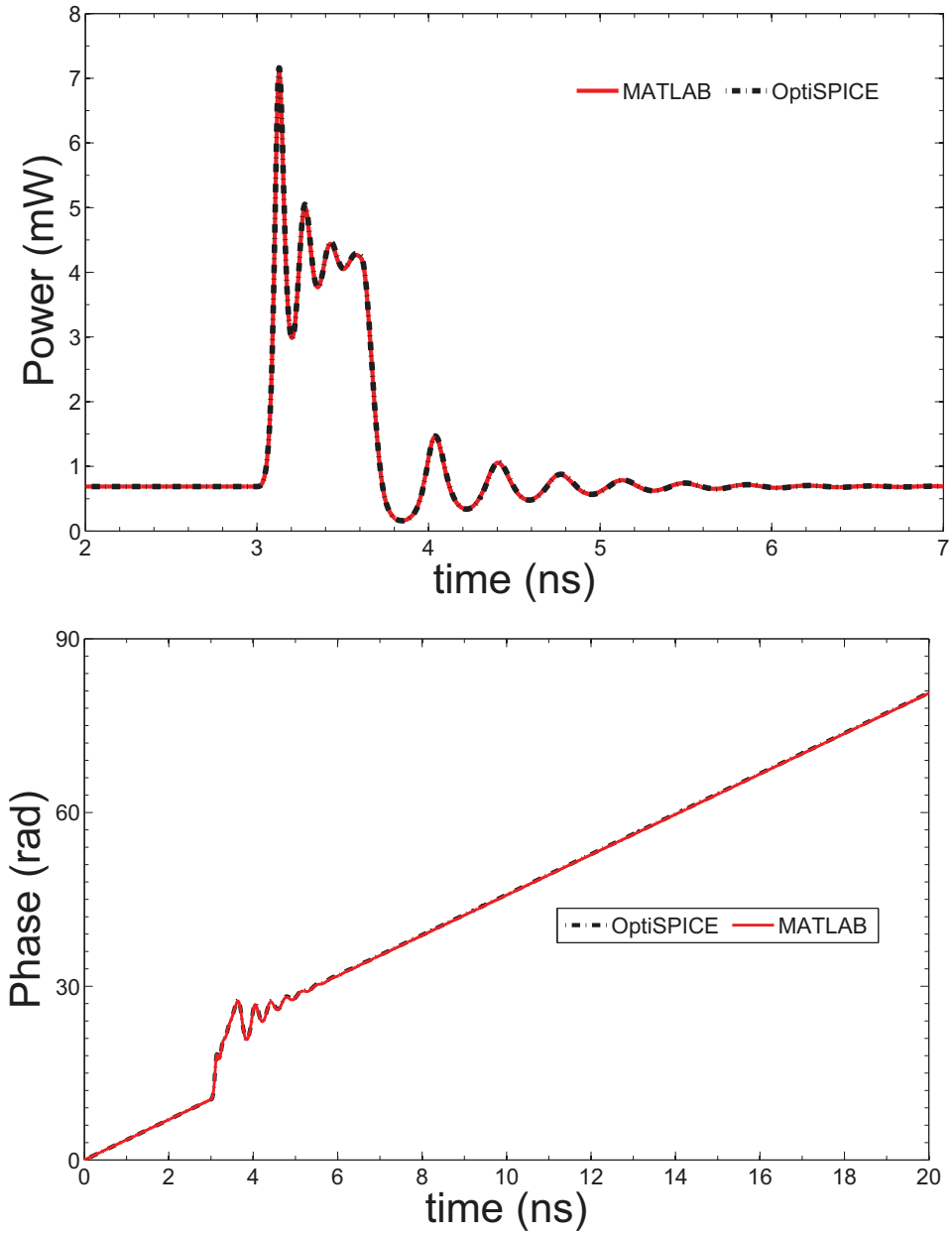

Figure 12: Output of the laser diode (a) magnitude of envelope signal (b) optical phase.

at the output of optical link. OptiSPICE results are also shown for comparison.

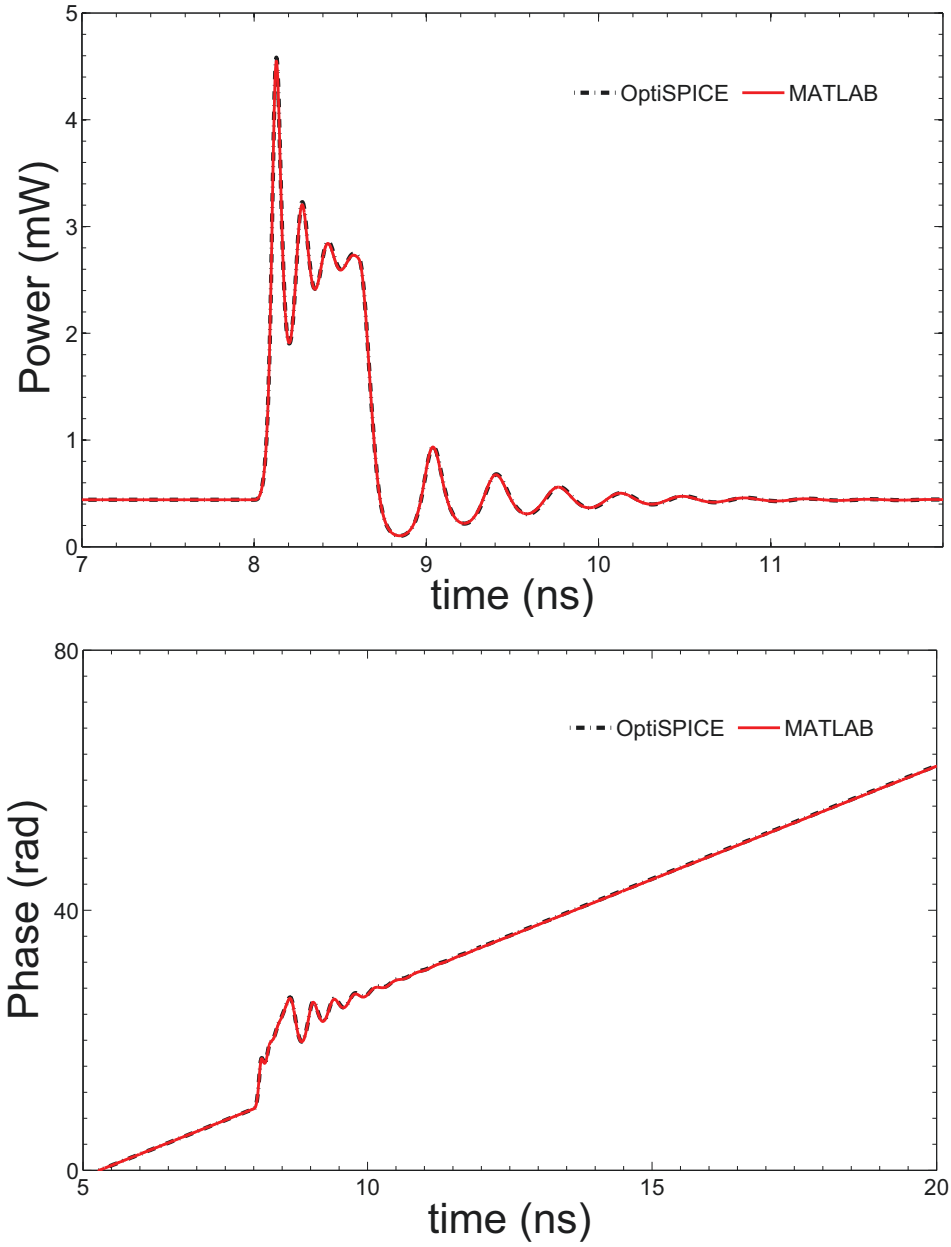

Figure 13: Output of the fiber (a) magnitude of envelope signal (b) optical phase.

3.4 Summary

This chapter presented an overview of the OptiSPICE simulator framework. In OptiSPICE the traditional MNA is extended to include optical signals by defining an optical node. Several optical component models developed for OptiSPICE such as

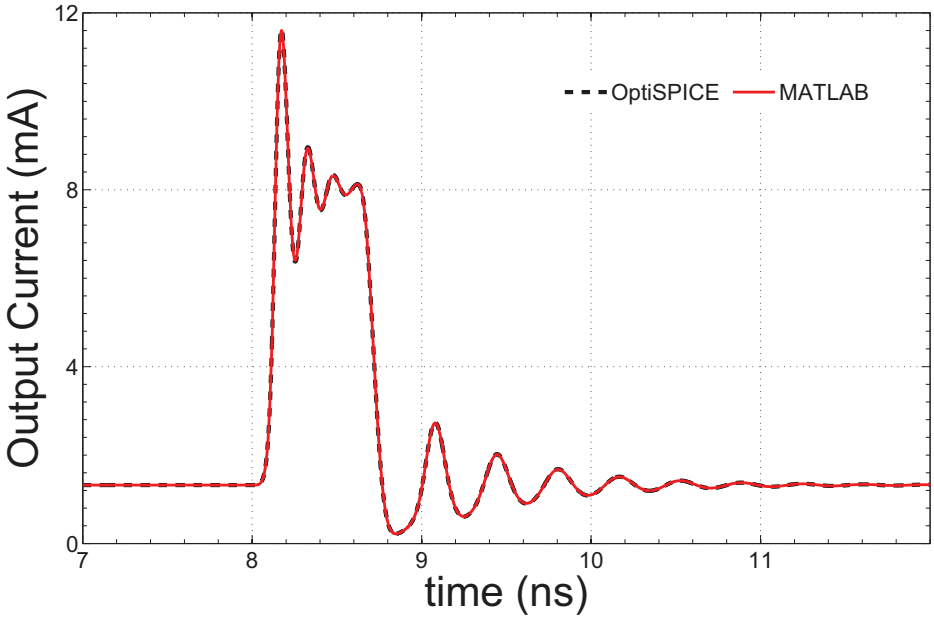

Figure 14: Current detected at the output of the optical link.

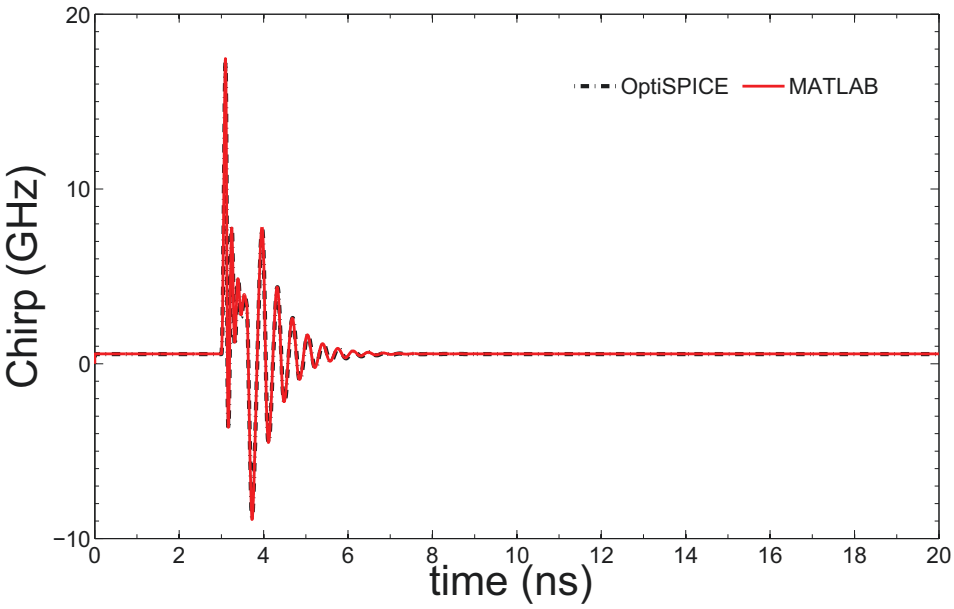

Figure 15: Chirp at the laser diode.

laser diode, multi-mode fiber and interference based devices have been described. The MATLAB implementation used in this thesis was compared to OptiSPICE to ensure its accuracy and validity. In order to use Harmonic Balance on a system containing

optical components models for optical devices are required. Models used in the proposed framework for interference based elements and photodiode are similar to those developed in this chapter, however, new models for optical fiber and in particular laser diode have to be made. The next chapter addresses the issues related to modeling optical signals in HB framework and develops the theory to overcome these issues.

Chapter 4

Steady-State Simulation of Microwave Photonic Systems using Harmonic Balance

There are several situations in which a steady-state simulation is sufficient to analyze system performance as is the case with typical circuits encountered in microwave photonics. Obtaining steady-state results using transient simulation is often time-consuming as the simulation needs to be run until all transients die down. Several techniques exist in literature to compute the steady-state solution of the system without the need to perform lengthy transient simulations. Of these methods Harmonic Balance (HB) is a widely used method for analog RF and microwave systems.

This chapter presents a technique to perform steady-state simulation of microwave photonic circuits consisting of optical and electrical components using Harmonic Balance considering the effect of phase on optical signals. The inclusion of this phase in a HB analysis raises several issues since optical phase is a non-periodic signal and HB assumes all system variables to be periodic. The theory developed in this paper highlights the problem of handling phase of optical signals in HB and presents a solution to overcome the issue. The chapter is organized as follows: Section 4.1 presents

the proposed method; it is followed with an explanation of the issues arising from the phase of optical signal especially in the case of the laser diode and develops the theory to overcome these issues. This is followed by a section presenting a model for an optical fiber operating in the linear regime that can be used with HB.

4.1 Basis of Proposed Method

The system equation for a general electrical circuit can be formulated using Modified Nodal Analysis (MNA) [24] as

$$\mathbf{G}\boldsymbol{x}(\mathbf{t}) + \mathbf{C}\frac{\boldsymbol{dx(t)}}{\boldsymbol{dt}} + \boldsymbol{f}(\boldsymbol{x(t)}) = \boldsymbol{b(t)} \tag{4.1}$$

where $\mathbf{G} \in \mathbb{R}^{n\times n}$ is the conductance matrix, $\mathbf{C} \in \mathbb{R}^{n\times n}$ represents the energy storage in elements, n is the number of system variables, $\boldsymbol{f}(\boldsymbol{x}(t)) \in \mathbb{R}^n$ is the vector representing current and charge contributions arising from nonlinear components, $\boldsymbol{b}(t) \in \mathbb{R}^n$ represents all the independent sources in the circuit, and $\boldsymbol{x(t)} \in \mathbb{R}^n$ is the vector of unknown system variables containing node voltages and necessary branch currents. Typically, this system of equations is solved in time domain using numerical integration techniques [25].

In OptiSPICE [23], traditional MNA [24] was extended to include optical components by defining an *Optical Node*. In this approach, the optical signal at each optical node is characterized by the magnitude and phase of the complex envelope for each mode within each channel (carrier frequency, ω_c) for the forward and backward direction of propagation [23]. As such, for a particular mode within a particular channel the magnitude ($E_F(t)$) and phase ($\varphi_F(t)$) in the forward direction, and the magnitude ($E_B(t)$) and phase ($\varphi_B(t)$) in the backward direction form the unknown system variables in $\boldsymbol{x(t)}$.

Harmonic Balance [26, 27] is one of several techniques used to find the steady-state response of the system directly without performing transient simulation. In HB, generally, the steady-state solution with respect to a multi-tone periodic excitation over a truncated set of frequencies using generalized Fourier series expansion is written as

$$\boldsymbol{x}(t) = \bar{\boldsymbol{X}}_o + \sum_{\lambda_k \epsilon \Lambda, \lambda_k \neq 0} \bar{\boldsymbol{X}}_k^c \cos(\lambda_k \mathbf{t}) + \bar{\boldsymbol{X}}_k^s \sin(\lambda_k \mathbf{t}) \tag{4.2}$$

where, Λ is the set of truncated frequencies, and $\bar{\boldsymbol{X}}_o$, $\bar{\boldsymbol{X}}_k^c$, $\bar{\boldsymbol{X}}_k^s$ are the vectors containing unknown coefficients required to be found in order to obtain the steady-state solution of the system. Following the regular procedure of HB [26, 27], (4.2) is substituted into (4.1) to obtain a set of nonlinear algebraic equations as

$$\mathbf{Y}\bar{\boldsymbol{X}} + \boldsymbol{F}(\bar{\boldsymbol{X}}) = \bar{\boldsymbol{B}} \tag{4.3}$$

where, $\mathbf{Y} \in \mathbb{R}^{n(2M+1)\times n(2M+1)}$ is a block diagonal matrix formed using MNA matrices, M is the number of truncated frequencies, $\bar{\boldsymbol{X}} \in \mathbb{R}^{n(2M+1)}$ is the unknown vector containing generalized Fourier series coefficients of $\boldsymbol{x}(t)$, $\boldsymbol{F}(\bar{\boldsymbol{X}}) \in \mathbb{R}^{n(2M+1)}$ represents nonlinearities, and $\bar{\boldsymbol{B}} \in \mathbb{R}^{n(2M+1)}$ represents generalized Fourier series coefficients of $\boldsymbol{b}(t)$. Typically, the nonlinear algebraic equations in (4.3) are solved using Newton-Raphson (NR) iterations [26, 27], (4.2). These iterations are performed by repeatedly solving

$$(\mathbf{Y} + \frac{\mathbf{dF}(\bar{\mathbf{X}}^{\mathbf{i}})}{\mathbf{dX}^{\mathbf{i}}})\boldsymbol{\Delta}\bar{\boldsymbol{X}}^{\mathbf{i}} = \mathbf{Y}\bar{\boldsymbol{X}}^{\mathbf{i}} + \boldsymbol{F}(\bar{\boldsymbol{X}}^{\mathbf{i}}) - \bar{\boldsymbol{B}} \tag{4.4}$$

where,

$$\boldsymbol{F}(\bar{\boldsymbol{X}}) = \boldsymbol{\Gamma}\rho^{\mathbf{T}}\boldsymbol{f}(\boldsymbol{X_s}) \tag{4.5}$$

$$\frac{\mathbf{dF}(\bar{\mathbf{X}})}{\mathbf{d}\bar{\mathbf{X}}} = \boldsymbol{\Gamma}\boldsymbol{\rho}^{\mathbf{T}}\frac{\mathbf{df}(\mathbf{X_s})}{\mathbf{dX_s}}\boldsymbol{\rho}\boldsymbol{\Gamma}^{-\mathbf{1}} \tag{4.6}$$

$$\boldsymbol{X_s} = \boldsymbol{\Gamma}^{-\mathbf{1}}\boldsymbol{\rho}\bar{\boldsymbol{X}} \tag{4.7}$$

where $\boldsymbol{\Gamma} \in \mathbb{R}^{n(2M+1)\times n(2M+1)}$ is the block diagonal DFT matrix, $\boldsymbol{\rho}$ is the permutation matrix for reordering equations [27], and $\boldsymbol{X}_s \in \mathbb{R}^{n(2M+1)}$ is the vector of response samples in the time domain evaluated at sampling time points

$$\bar{\boldsymbol{t}}_{\boldsymbol{s}} = \begin{bmatrix} t_o & t_1 & \cdots & t_{2M} \end{bmatrix}^T \qquad for \qquad 0 \leq t_i < T_{global} \tag{4.8}$$

where T_{global} is the global time period of an almost-periodic (AP) signal related to the smallest frequency component in Λ [26, 27].

When using HB on a system containing optical components, models for optical devices such as laser diode, optical fiber, photodiode, and interference based elements are required. Models used in the proposed framework for interference based elements and photodiode are similar to those developed in OptiSPICE, however, models for optical fiber and in particular laser diode have to be readdressed especially due to the non-periodic nature of optical phase that is generated in the element.

The following section highlights the problem of handling phase of optical signals in conjunction with HB and presents a solution to overcome the issue.

4.2 Diode Laser

A physically based model for a single mode laser diode is given as

$$\frac{dN}{dt} = -\frac{N}{\tau_n} - g_0(N - N_t)\frac{S}{1+\epsilon S} + \frac{I_D - I_{off}(T)}{qV_L} \tag{4.9}$$

$$\frac{dS}{dt} = \frac{\gamma\beta N}{\tau_n} - \frac{S}{\tau_p} + \gamma g_o(N - N_t)(\frac{S}{1+\epsilon S}) \tag{4.10}$$

$$\frac{d\varphi}{dt} = \frac{1}{2}\alpha\gamma g_o(N - N_t) - \frac{\alpha}{2\tau_p} \tag{4.11}$$

where $N(t)$ and $S(t)$ are the laser carrier and photon density respectively, $\varphi(t)$ represents the optical phase, I_D is the efficient injected current, V_L is the laser volume, q is the electron charge, ϵ is the gain comparison factor, τ_n and τ_p are the electron and photon lifetimes, γ is the mode confinement factor, β is the spontaneous emission coefficient, g_o is the gain coefficient, N_t is the carrier density at transparency, α is the linewidth enhancement factor, and $I_{off}(T)$ models the temperature dependent nature of the laser. Further, the complex optical signal at the laser output is found as

$$E_r(t) = E_o(t)\cos(\omega_c t + \varphi(t)) \tag{4.12}$$

$$E_i(t) = E_o(t)\sin(\omega_c t + \varphi(t)) \tag{4.13}$$

where $E_r(t)$ and $E_i(t)$ are the real and imaginary parts of the optical signal, $E_o(t)$ is the optical signal magnitude linearly proportional to the square root of the photon density ($S(t)$), and ω_c represents the optical carrier frequency. As will be clarified shortly, the laser optical phase variable is not periodic, therefore, it cannot be directly used as a system variable in the traditional truncated HB framework. The rest of this section presents a technique to include the effect of optical phase in HB framework without directly using it as a system variable.

The optical phase can be derived by integrating (4.11) on both sides as

$$\varphi(t) = \int_0^t \frac{d\varphi}{d\tau} d\tau = \frac{\alpha}{2}(\gamma g_o \int_0^t N(\tau)d\tau - (\frac{1}{\tau_p} + \gamma g_o N_t)t) \tag{4.14}$$

assuming $\varphi(0) = 0$ without loss of generality. As mentioned earlier, in HB, the response of the circuit corresponding to a multi-tone excitation is found using generalized Fourier series transform. For instance, the laser carrier density ($N(t)$) at

steady-state over a frequency truncation can be written as

$$N(t) = a_o^N + \sum_{\lambda_k \epsilon \Lambda, \lambda_k \neq 0} a_k^{N^c} \cos(\lambda_k t) + a_k^{N^s} \sin(\lambda_k t) \tag{4.15}$$

where a_o^N is the DC coefficient and $a_k^{N^c}$ and $a_k^{N^s}$ are the cosine and sine coefficients of the laser carrier density corresponding to the k_{th} truncated frequency respectively. Substituting (4.15) into (4.14) and performing integration, the optical phase can be found as the summation of a almost-periodic function and a ramp function as

$$\varphi(t) = PF(t) + K^{'} t \tag{4.16}$$

where,

$$K^{'} = \frac{\alpha}{2}(\gamma g_o a_o^N - \gamma g_o N_t - \frac{1}{\tau_p}) \tag{4.17}$$

$$PF(t) = \frac{\alpha \gamma g_o}{2} \sum_{\lambda_k \epsilon \Lambda, \lambda_k \neq 0} \frac{a_k^{N^s}}{\lambda_k}(1 - \cos(\lambda_k t)) + \frac{a_k^{N^c}}{\lambda_k} \sin(\lambda_k t) \tag{4.18}$$

The non-periodic nature of the optical phase manifests as a ramp function that occurs in the second term in (4.16).

Substituting (4.16) into (4.12) and (4.13), the complex field at the laser output can be written as

$$E_r(t) = E_o(t) \cos(PF(t) + Kt) \tag{4.19}$$

$$E_i(t) = E_o(t) \sin(PF(t) + Kt) \tag{4.20}$$

where,

$$K = \omega_c + K^{'} \tag{4.21}$$

Note that due to the periodic property of sinusoidal functions, (4.19) and (4.20) are almost-periodic with respect to K despite the phase of the optical signal being non-periodic. As a result, the K term can be treated as a new tone in the system

which can be added to the set of truncated frequencies in the HB formulation.

When implementing HB using K as a new tone, time-domain samples in (4.5) and (4.6) corresponding to E_r and E_i need to be evaluated. These are found at given time points in $\bar{\boldsymbol{t}}_s$ as

$$\boldsymbol{E_r^s} = \begin{bmatrix} E_r(t_o) & E_r(t_1) & \cdots & E_r(t_{2M}) \end{bmatrix}^T \tag{4.22}$$

$$\boldsymbol{E_i^s} = \begin{bmatrix} E_i(t_o) & E_i(t_1) & \cdots & E_i(t_{2M}) \end{bmatrix}^T \tag{4.23}$$

where,

$$E_r(t_i) = E_o(t_i)\cos(PF(t_i) + Kt_i) \tag{4.24}$$

$$E_i(t_i) = E_o(t_i)\sin(PF(t_i) + Kt_i) \tag{4.25}$$

This enables the inclusion of the effect of the optical phase in the system equations without introducing the non-periodic optical phase as one of the system variables.

In order to explain a further issue in modeling optical phase, consider a simple case where the HB system of equations is formed using Λ as $\{0, \omega, K, K \pm \omega\}$ in which ω is the fundamental frequency of system excitation. The $\mathbf{Y}$ matrix is found as

$$\mathbf{Y} = \begin{bmatrix} \mathbf{G} & 0 & 0 & 0 & 0 & 0 & 0 & 0 & 0 \\ 0 & \mathbf{G} & \omega\mathbf{C} & 0 & 0 & 0 & 0 & 0 & 0 \\ 0 & -\omega\mathbf{C} & \mathbf{G} & 0 & 0 & 0 & 0 & 0 & 0 \\ 0 & 0 & 0 & \mathbf{G} & K\mathbf{C} & 0 & 0 & 0 & 0 \\ 0 & 0 & 0 & -K\mathbf{C} & \mathbf{G} & 0 & 0 & 0 & 0 \\ 0 & 0 & 0 & 0 & 0 & \mathbf{G} & (K+\omega)\mathbf{C} & 0 & 0 \\ 0 & 0 & 0 & 0 & 0 & -(K+\omega)\mathbf{C} & \mathbf{G} & 0 & 0 \\ 0 & 0 & 0 & 0 & 0 & 0 & 0 & \mathbf{G} & (K-\omega)\mathbf{C} \\ 0 & 0 & 0 & 0 & 0 & 0 & 0 & -(K-\omega)\mathbf{C} & \mathbf{G} \end{bmatrix} \tag{4.26}$$

As seen, the $\mathbf{Y}$ matrix contains K which in turn contains a_0^N which is one of the system variables in $\bar{\boldsymbol{X}}$. These system variables have to be extracted from the $\mathbf{Y}$ matrix and absorbed into the nonlinear vector. This results in a modification to the system of equations and the new system of equations can be written as

$$\mathbf{Y}^{'}\bar{\boldsymbol{X}} + \boldsymbol{F}^{'}(\bar{\boldsymbol{X}}) = \boldsymbol{B}, \tag{4.27}$$

in which,

$$\boldsymbol{F}^{'}(\bar{\boldsymbol{X}}) = \boldsymbol{F}(\bar{\boldsymbol{X}}) + \frac{\alpha}{2}\gamma g_o a_o^N \begin{bmatrix} 0 \\ 0 \\ 0 \\ \mathbf{C}\bar{\boldsymbol{X}}_2^s \\ -\mathbf{C}\bar{\boldsymbol{X}}_2^c \\ \mathbf{C}\bar{\boldsymbol{X}}_3^s \\ -\mathbf{C}\bar{\boldsymbol{X}}_3^c \\ \mathbf{C}\bar{\boldsymbol{X}}_4^s \\ -\mathbf{C}\bar{\boldsymbol{X}}_4^c \end{bmatrix}, \tag{4.28}$$

$$\mathbf{Y}^{'} = \begin{bmatrix} \mathbf{G} & 0 & 0 & 0 & 0 & 0 & 0 & 0 & 0 \\ 0 & \boldsymbol{G} & \omega\mathbf{C} & 0 & 0 & 0 & 0 & 0 & 0 \\ 0 & -\omega\mathbf{C} & \mathbf{G} & 0 & 0 & 0 & 0 & 0 & 0 \\ 0 & 0 & 0 & \boldsymbol{G} & k_\varphi\mathbf{C} & 0 & 0 & 0 & 0 \\ 0 & 0 & 0 & -k_\varphi\mathbf{C} & \mathbf{G} & 0 & 0 & 0 & 0 \\ 0 & 0 & 0 & 0 & 0 & \mathbf{G} & (k_\varphi+\omega)\mathbf{C} & 0 & 0 \\ 0 & 0 & 0 & 0 & 0 & -(k_\varphi+\omega)\mathbf{C} & \mathbf{G} & 0 & 0 \\ 0 & 0 & 0 & 0 & 0 & 0 & 0 & \mathbf{G} & (k_\varphi-\omega)\mathbf{C} \\ 0 & 0 & 0 & 0 & 0 & 0 & 0 & -(k_\varphi-\omega)\mathbf{C} & \mathbf{G} \end{bmatrix}, \tag{4.29}$$

and,

$$k_\varphi = \omega_c - \frac{\alpha}{2}(\gamma g_o N_t + \frac{1}{\tau_p}) \tag{4.30}$$

where $\bar{\boldsymbol{X}}_i^s$ and $\bar{\boldsymbol{X}}_i^c \in \mathbb{R}^n$ are the vectors of sine and cosine coefficients corresponding to the i_{th} truncated frequency respectively.

The laser thus consists of an electrical diode and rate equations in addition to a new tone and added nonlinearities to model the non-periodic nature of the optical phase.

4.3 Linear Fiber Model

Over short distances, optical fibres and waveguides can be treated as linear devices and modeled using delay elements and attenuation [23, 68, 69]. At steady-state however, the time delay in the optical fiber manifests itself as a phase shift. For HB, the input/output relationship incorporating this phase shift can be modeled for the optical waveguide over a set of truncated frequencies (Λ) along with attenuation as

$$\begin{bmatrix} X_0{}' \\ X_1^{c\prime} \\ X_1^{s\prime} \\ X_2^{c\prime} \\ X_2^{s\prime} \\ \vdots \\ \vdots \\ X_M^{c}{}' \\ X_M^{s}{}' \end{bmatrix} = A_0 \begin{bmatrix} 1 & 0 & 0 & \cdots & 0 & 0 \\ 0 & \mathbf{A_1^{2\times 2}} & 0 & \cdots & \cdots & 0 \\ 0 & 0 & \mathbf{A_2^{2\times 2}} & 0 & \cdots & 0 \\ \vdots & \vdots & 0 & \ddots & \ddots & \vdots \\ \vdots & \vdots & \vdots & \ddots & \ddots & \vdots \\ 0 & 0 & 0 & \cdots & 0 & \mathbf{A_M^{2\times 2}} \end{bmatrix} \begin{bmatrix} X_0 \\ X_1^c \\ X_1^s \\ X_2^c \\ X_2^s \\ \vdots \\ \vdots \\ X_M^c \\ X_M^s \end{bmatrix} \tag{4.31}$$

where M is the number of truncated frequencies, $X_0/X_0^{'}$ are the fiber input/output dc coefficients, $X_i^s/X_i^{s'}$ and $X_i^c/X_i^{c'}$ respectively are the input/output sine and cosine coefficients corresponding to the i_{th} truncated frequency, A_0 is the fiber attenuation, and

$$\mathbf{A_i} = \begin{bmatrix} \cos(\lambda_i \tau_d) & -\sin(\lambda_i \tau_d) \\ \sin(\lambda_i \tau_d) & \cos(\lambda_i \tau_d) \end{bmatrix} \tag{4.32}$$

where λ_i is the i_{th} truncated frequency and τ_d is the time delay proportional to the length of the fiber. The derivation of (4.32) is provided in Appendix A.

In the presence of a laser diode which introduces a new tone (K) in the proposed HB system of equations, an approach similar to that presented in the previous subsection is necessary to extract a_0^N (one of the system variables) from $\mathbf{Y}$ and absorb it into the nonlinear vector. For example, the input/output relationship of an optical waveguide for $\Lambda = \{0, \omega, K\}$ can be written as

$$\boldsymbol{X_f^{'}} = \mathbf{A}\boldsymbol{X_f} + \boldsymbol{F_d}(\bar{\boldsymbol{X}}) \tag{4.33}$$

where $\boldsymbol{X_f}$ and $\boldsymbol{X_f^{'}}$ are the vectors containing Fourier coefficients at the input and output of the fiber respectively and

$$\mathbf{A} = A_0 \begin{bmatrix} 1 & 0 & 0 & 0 & 0 \\ 0 & \cos(\omega\tau_d) & -\sin(\omega\tau_d) & 0 & 0 \\ 0 & \sin(\omega\tau_d) & \cos(\omega\tau_d) & 0 & 0 \\ 0 & 0 & 0 & 0 & 0 \\ 0 & 0 & 0 & 0 & 0 \end{bmatrix} \tag{4.34}$$

and

$$\boldsymbol{F_d}(\bar{\boldsymbol{X}}) = \begin{bmatrix} 0 \\ 0 \\ 0 \\ X_2^c \cos(k_\varphi \tau_d) - X_2^s \sin(k_\varphi \tau_d) \\ X_2^c \sin(k_\varphi \tau_d) + X_2^s \cos(k_\varphi \tau_d) \end{bmatrix} \cos(\frac{\alpha \gamma g_o}{2} a_o^N \tau_d)$$
$$+ \begin{bmatrix} 0 \\ 0 \\ 0 \\ -X_2^c \sin(k_\varphi \tau_d) - X_2^s \cos(k_\varphi \tau_d) \\ X_2^c \cos(k_\varphi \tau_d) - X_2^s \sin(k_\varphi \tau_d) \end{bmatrix} \sin(\frac{\alpha g_o \gamma}{2} a_o^N \tau_d) \quad (4.35)$$

This nonlinear input/output relationship can now be stamped into the HB system of equations to model the effects of attenuation and phase-shift observed in an optical waveguide.

4.4 Summary

This chapter presented a technique to perform steady-state simulation of microwave photonic systems. The first section presented the proposed method and is followed with a descriptation of issues arising from inclusion of the non-periodic optical phase generated in typical optical sources in a HB simulation framework. A theory was developed in this chapter to include the effect of this non-periodic phase by using the real and imaginary parts of the complex optical signal. The models for laser diode and optical fiber were developed in order to be used in the HB framework. The next chapter provides three numerical examples to illustrate the feasibility of the proposed method.

Chapter 5

Numerical Results

In order to demonstrate the practicality of the proposed method three examples are presented. Results from the proposed method are compared to published results and OptiSPICE [23] where possible. The first example presents an analog RoF link, the second example captures the heterodyning behavior at optical detectors used in optical generation of microwave/RF signals, and the third example presents an electrical feedback controlled optical link.

5.1 Radio over Fiber (RoF) Link

RoF is a technique allowing RF signals to be directly transmitted through an optical fiber. Traditionally, a simple RoF link constitutes of an optical source, modulator, optical fiber, and photodetector. When using the direct modulation technique typically the RF signal is connected via a bias tee connection to the laser diode demonstrated in Fig. 16. In this example, a sinusoidal current oscillating at 10 GHz with a DC value of 42 mA and a total peak to peak current of 11 mA drives the laser diode. The proposed method was used to obtain the magnitude and phase of the frequency components defined for each system variable in the formulation. The results obtained from this method were compared to that of OptiSPICE. The link parameters used in

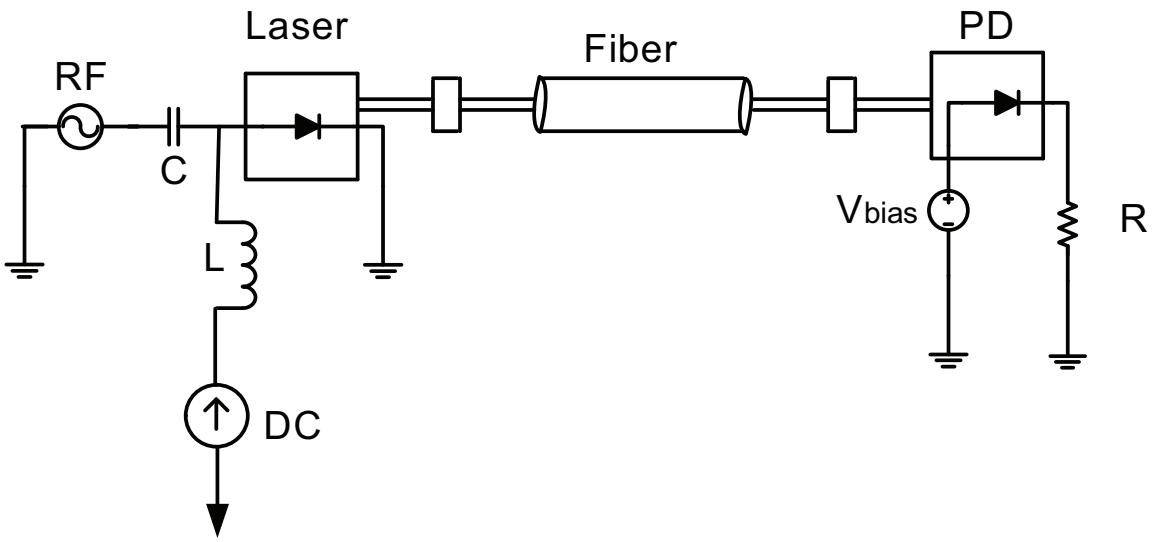

Figure 16: Radio over Fiber link schematic with laser driver and detector.

the simulation are provided in Table 4. OptiSPICE being a transient simulator had to be run for a substantial length of time until the transients die down to obtain the steady-state results. Fig. 17 presents simulation results in the time domain for the laser diode driving current along with a comparison using the result from OptiSPICE. As seen, the two simulators predict the same response at steady-state.

Fig. 18 shows the real and imaginary parts of the envelope of the optical signal at the output of the laser diode. The response obtained from OptiSPICE is also shown for comparison. As demonstrated, the real and imaginary parts of the envelope are almost-periodic with respect to the modulation frequency and the new tone introduced by the non-periodic nature of the optical phase. Note that the time scale used in these figures is different from the time scale used in Chapter 3 since in this example the excitation frequency is different and also the steady-state response is of interest as opposed to the transient response.

Fig. 19 presents results corresponding to the envelope at the input and output of the optical fiber. The response obtained from OptiSPICE is also shown for comparison. As seen, the input of the optical fiber is the same as the output of the laser

Table 4: Optical link parameters

Parameter	Value	Unit
V_L	1.5×10^{-10}	cm^3
γ	.4	-
g_0	21.57×10^{-7}	cm^3/s
ϵ	1×10^{-17}	cm^3
q	1.6×10^{-19}	A×s
τ_p	3	ps
τ_n	1	ns
β	3×10^{-5}	-
N_t	1×10^{18}	cm^{-3}
c	3×10^8	m/s
A_0	.8	-
τ_d	.2	ns

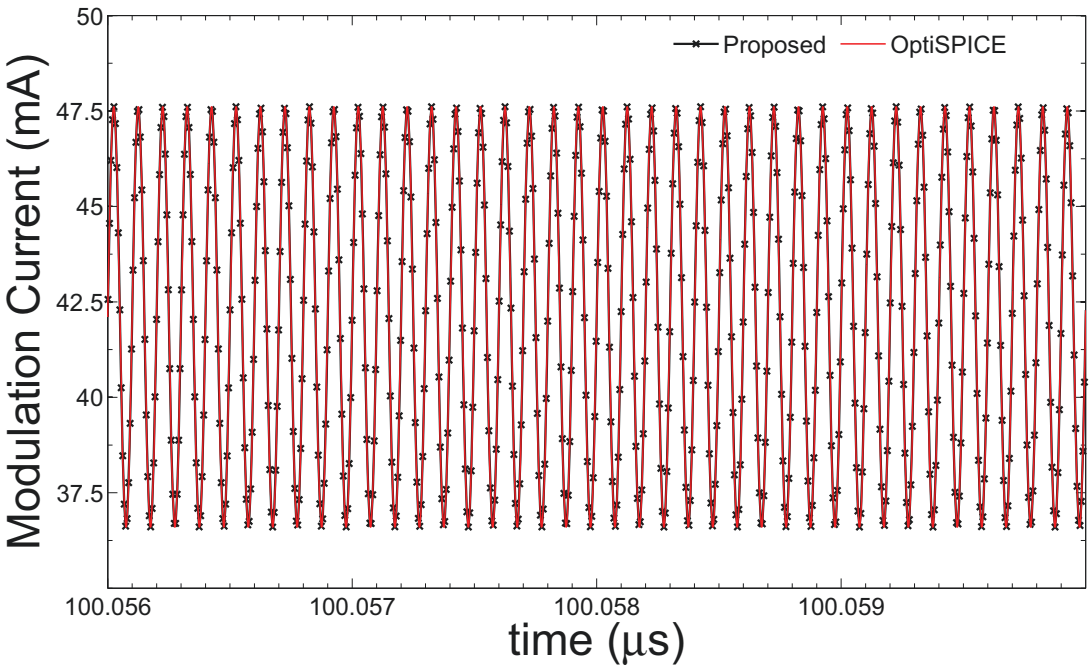

Figure 17: Modulation current driving the laser diode.

diode. This signal passes through the optical fiber where it encounters attenuation and phase shift as presented in Fig. 19.

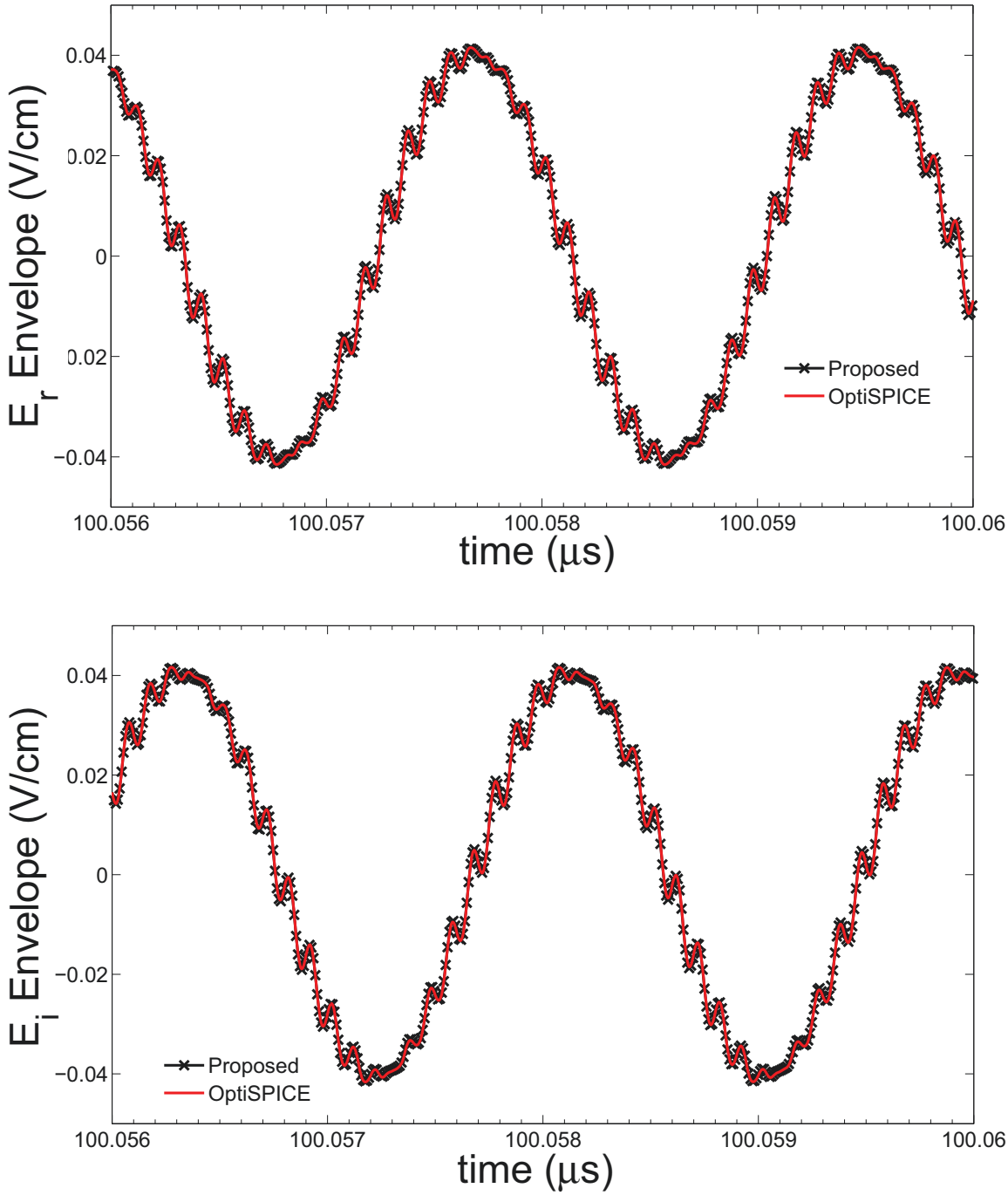

Figure 18: Real and imaginary parts of the envelope of optical field at the laser output.

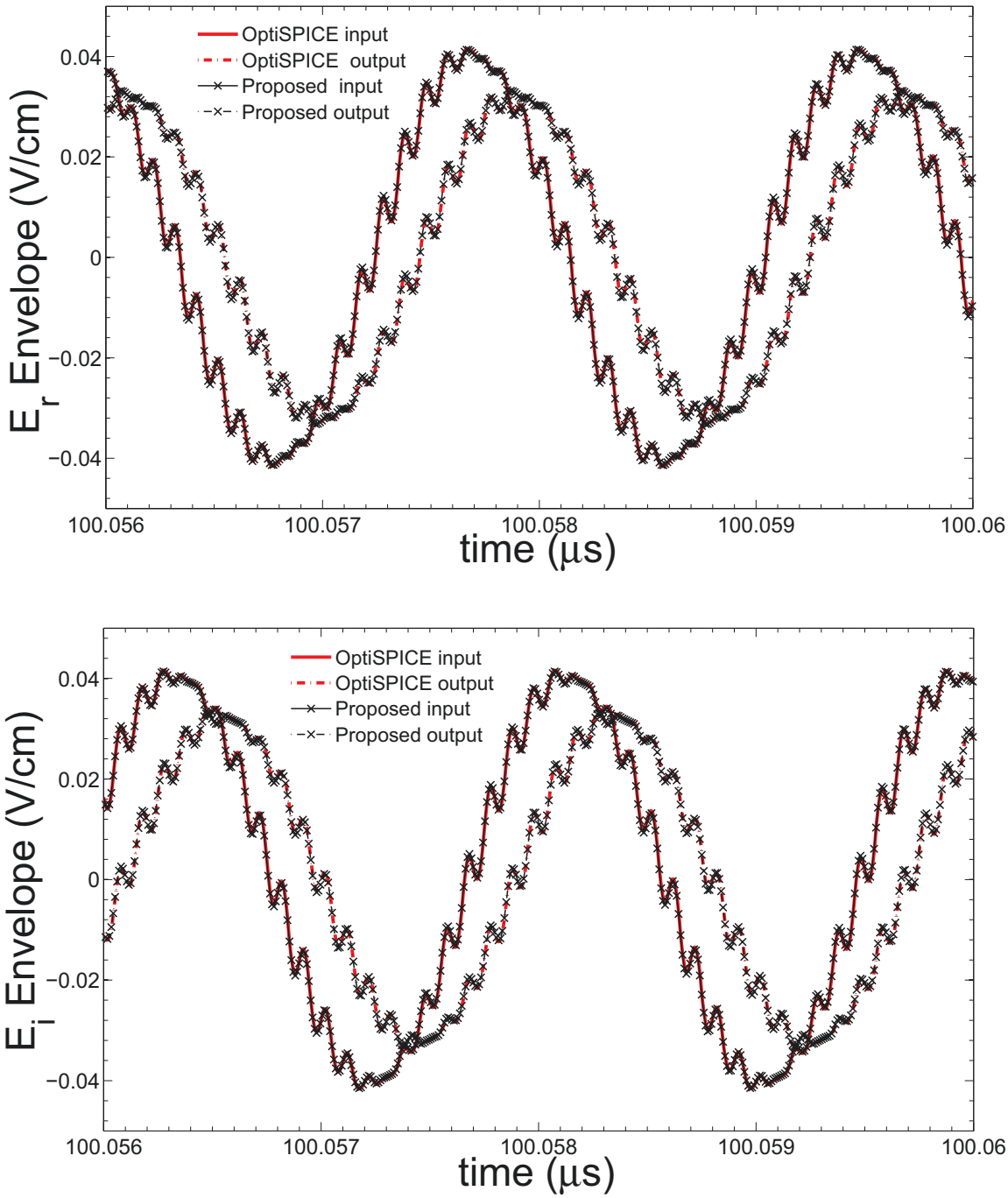

Figure 19: Real and imaginary parts of the envelope field at input/output of the optical fiber.

5.2 Optical Heterodyning Link

This subsection presents an example where optical heterodyning occurs between two optical signals operating at different wavelengths. Generally, optical heterodyning

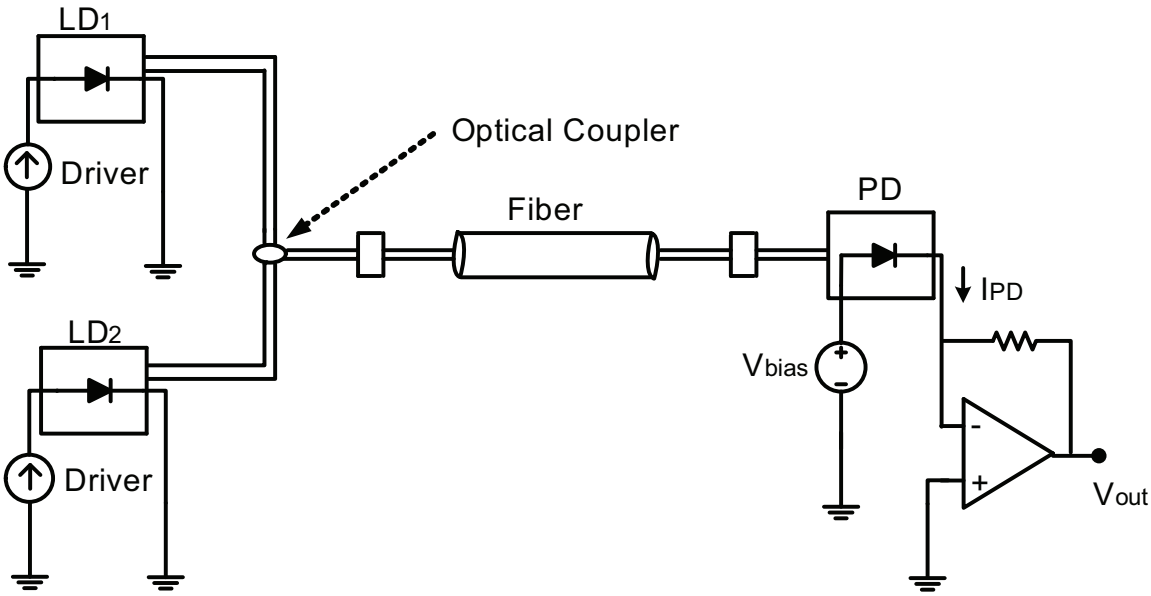

Figure 20: Optical link mixing of two optical waves to generate a microwave/RF signal.

at the photodiode generates an electrical signal with a frequency corresponding to the wavelength spacing of the optical signals [1, 2]. Fig. 20 shows the schematic of the optical circuit considered to demonstrate the heterodyning effect used for optical generation of microwave/RF signals.

In this circuit the 1319nm laser diodes have almost identical driving circuits emitting light at 10mW with .1nm separation between their wavelengths. The link parameters used in the simulation are provided in Table 4. The output of the laser diodes are coupled into an optical fiber which in turn is connected to a photodiode.

Theoretically, a microwave signal of 17.24GHz is expected at the output of the photodiode due to heterodyning [1, 2]. This optical circuit is simulated using the proposed method. Fig. 21 shows the magnitude of the frequency components of the optical field at the output of both laser diodes obtained from the simulation and as expected are separated by 17.24GHz.

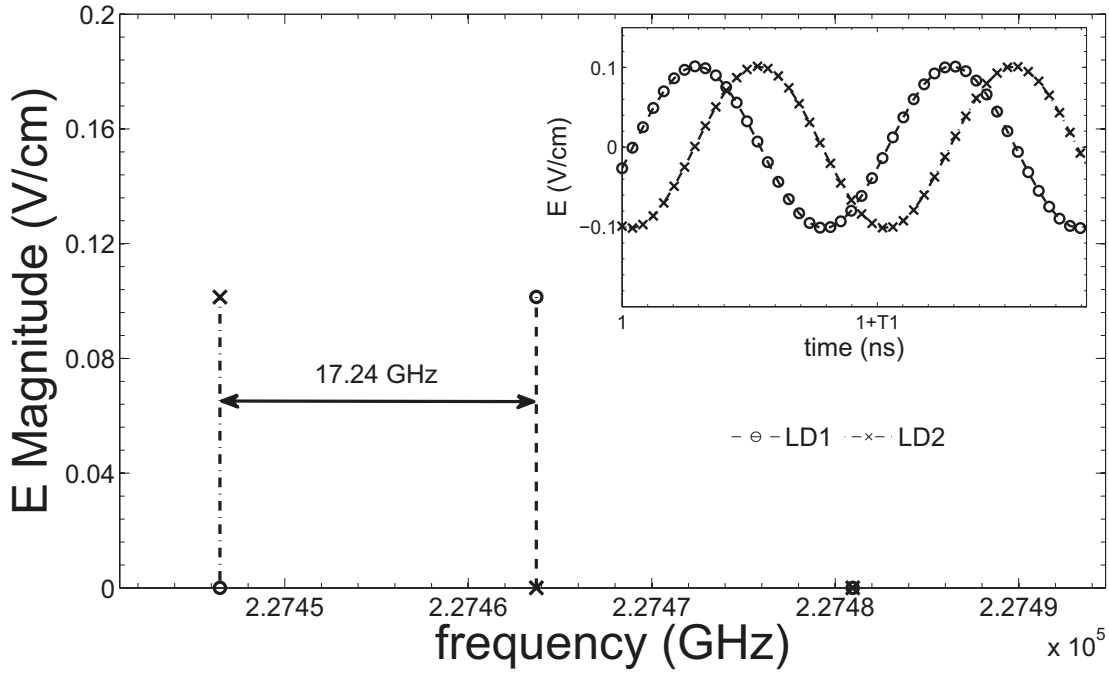

Figure 21: Magnitude of the optical field at the output of laser diodes. The inset figure shows the output in the time domain plotted after 1ns. T1: Time period of the optical carrier of LD1.

Fig. 22 presents the simulation results obtained for the output (V_{out}) and as expected the frequency of the generated microwave signal is 17.24 GHz.

5.3 Laser Frequency Stabilization using Electrical Feedback

In several situations designers observe a frequency drift over time in laser diodes caused by system fluctuations [2] resulting in a frequency shift of the generated microwave/RF signal through heterodyning. The unwanted drift typically can be compensated using an electrical feedback circuit to generate an error signal corresponding to the frequency drift by comparing the output of the link to a stable local RF oscillator as demonstrated in Fig. 23. The mixer output then is followed by a low-pass

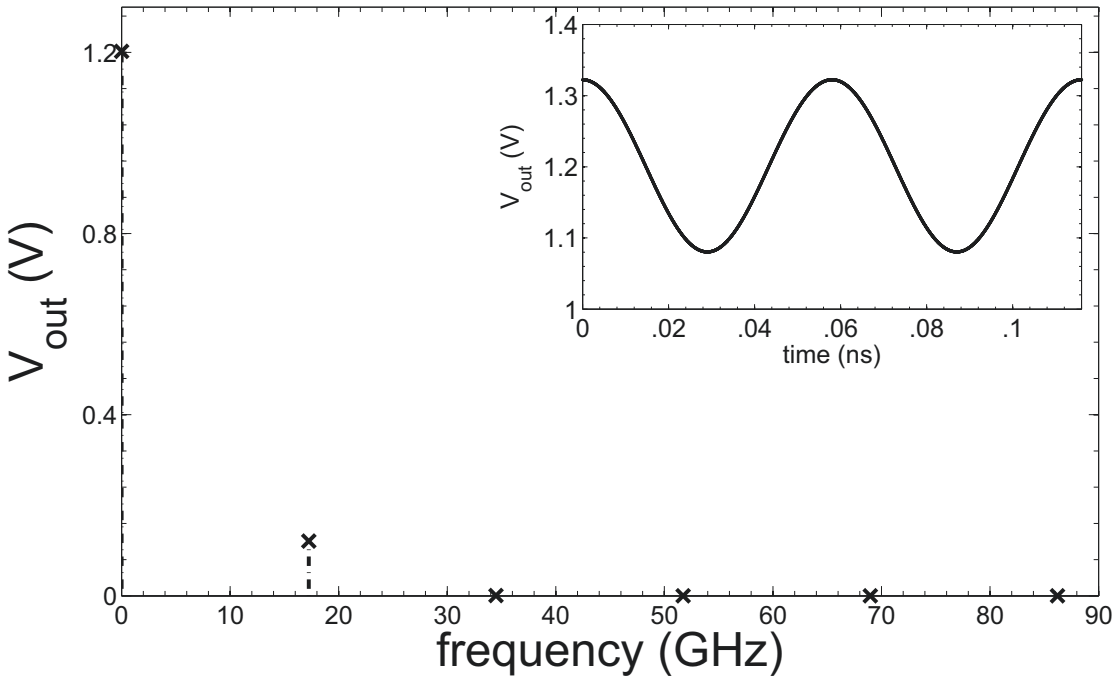

Figure 22: Magnitude of the voltage detected at the output. Inset figure shows the microwave signal generated at the output in the time domain.

loop filter which generates an error signal proportional to the frequency difference between the beat note and the reference oscillator. The feedback circuit is designed such that the current driving the laser is decreased if the laser has a positive drift and is increased if there is a negative drift.

In this example, the lasers are operating at the same power emitting light separated by a frequency of 10MHz. The link parameters used in the simulation are provided in Table 4. The link is formulated and simulated using the proposed technique for three different cases: 1) ideal case where there is no drift in the laser diodes, 2) case where there is a 10kHz drift in one of the laser diodes while the feedback circuit is disconnected, and 3) case where there is the same 10kHz drift while the feedback circuit is connected.

Results for the three cases are presented in Figs. 11, 12 and are discussed below:

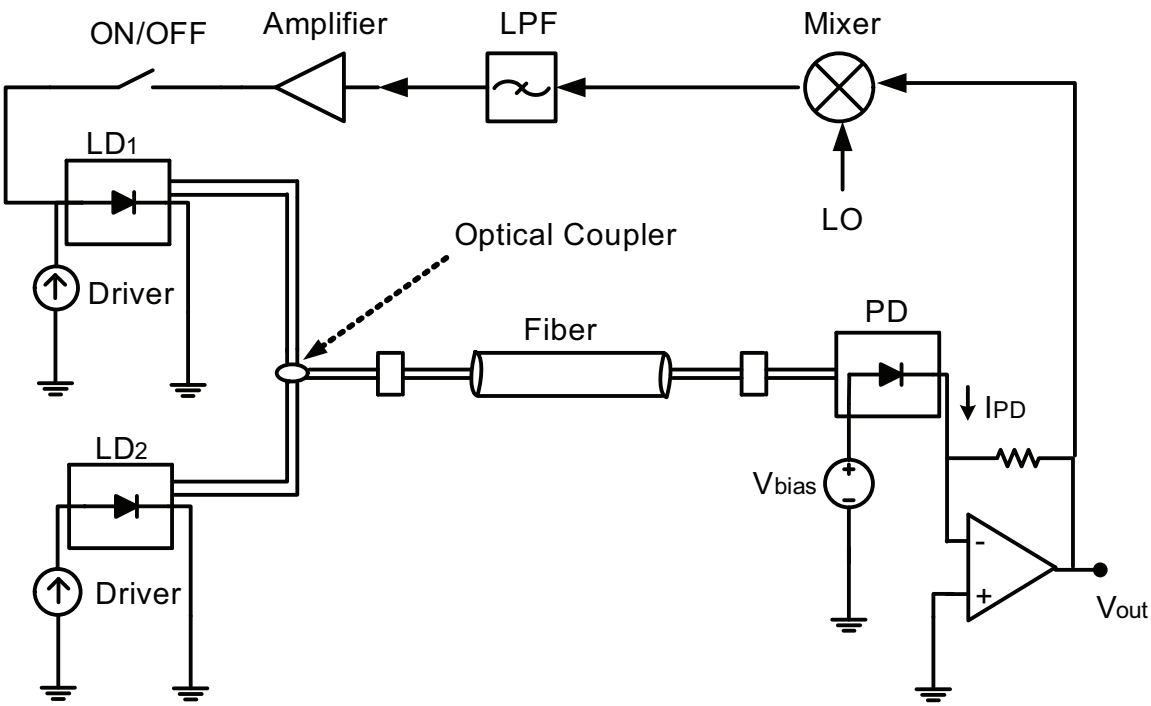

Figure 23: Laser frequency Stabilization link schematic. LPF: Low Pass Filter.

Case 1: As seen, frequencies of the output optical signal of the lasers are separated by 10MHz as expected and a steady-state 10MHz electrical microwave signal is observed at V_{out}.

Case 2: As shown in the figures, the frequency drift of LD1 resulted in a 10 kHz frequency shift in the output optical signal of LD1. This leads to a corresponding shift in the frequency of the microwave signal generated at V_{out}. This shift in the microwave signal is an undesirable effect and needs to be eliminated.

Case 3: With the feedback circuit turned on, the frequency shift in the output optical signal of LD1 due to its drift is eliminated aligning its frequency with the frequency observed in Case 1. The electrical microwave signal generated at V_{out} shows no shift in this case and produces the desired 10 MHz signal.

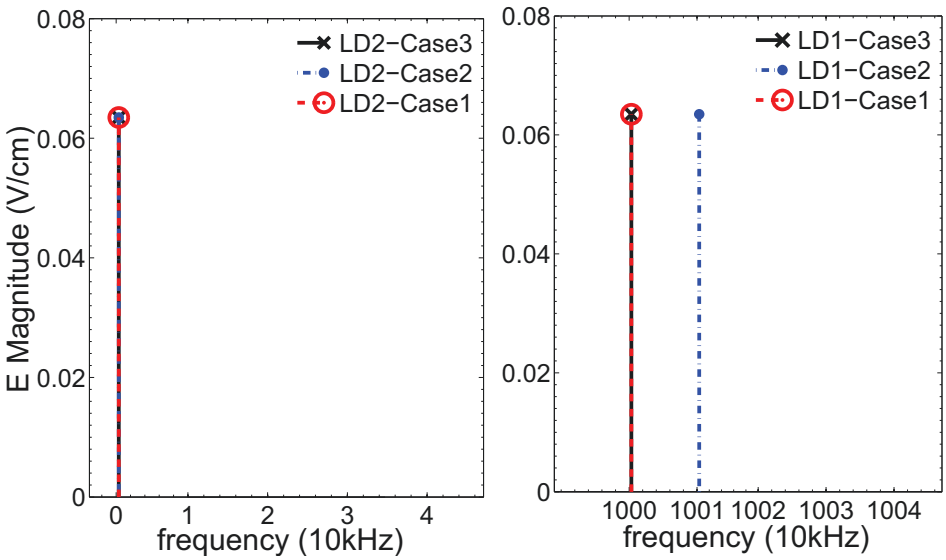

Figure 24: Magnitude of the frequency components of the optical field at the output of laser diodes. Left figure corresponds to LD2 and right figure corresponds to LD1 (in order to plot these figures the frequency axis was shifted to 224THz to notice the 10KHz frequency drift).

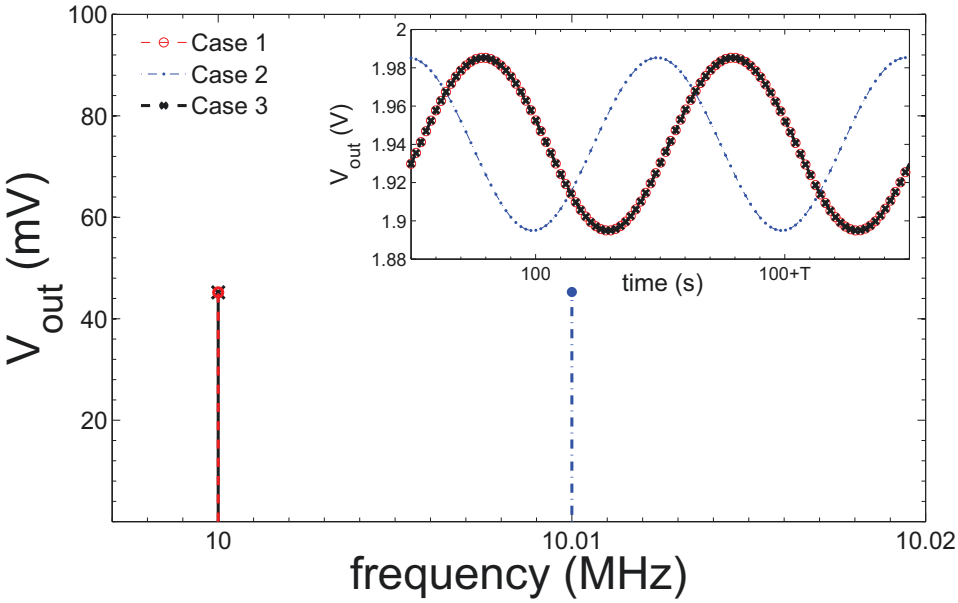

Figure 25: Magnitude of the frequency components at the output (V_{out}) for each of the cases. The inset figures shows the steady-state response in time domain (the time is chosen arbitrarily large to capture the frequency drifts between cases).

5.4 Summary

In this chapter, the performance and accuracy of the proposed method for some practical examples have been demonstrated. The first example presented an RoF link in which an RF signal is transmited through an optical fiber. The second example captured the hetrodyning behavior of photodiode used for optical generation of microwave signals. The last example presented an optical link in which the electrical error signal generated at the output of the link is used to remove the unwanted frequency drift in laser diode. Results obtained from proposed method were compared with theory and published methods where possible.

Chapter 6

Conclusion and Future Work

6.1 Summary

As the use of optical devices for applications such as generation, distribution, process, and control of microwave signals [1–9] expands, there will be need for a self-consistent microwave photonic system simulator. In recent past, several tools [10–22] have been introduced for simulation of optoelectronic systems. Most of these approaches do not pay a particular attention to the optical phase which is an important parameter for modeling interference effects in optical systems.

Recently, OptiSPICE [23] presented a self-consistent transient optoelectronic circuit simulator considering the effect of optical phase on optical signals. In this framework, the complex optical signal is mapped into the MNA formulation by defining an *optical node* [23]. In this method, an optical signal in each mode within a particular channel is represented by four state variables, the magnitude and phase of the forward and reverse traveling signals [23]. A brief overview of OptiSPICE simulation approach for modeling optical signals was provided in the third chapter of this thesis.

Though a transient simulation provides a good grasp of system behavior, there are several situations in which a steady-state solution is sufficient to investigate the system behavior. In these situations, generally, the high computation time required for

conventional transient simulation to capture the steady-state solution can be avoided by using steady-state techniques. In Chapter 2, a brief background of traditional steady-state simulation methods is presented with emphasises on Harmonic Balance which to the date is the method of choice for simulating analog microwave systems.

In Chapter 4, using Harmonic Balance [26,27], a technique is presented to perform steady-state simulation of microwave photonic circuits where optical and electrical components co-exist at the same design level. One of the challenges faced in developing this technique was related to modeling the effect of non-periodic optical phase on the overall system. This issue was addressed by developing the theory to use real and imaginary parts of the complex optical signal as system variables which encapsulate the effect of the non-periodic optical phase while being almost-periodic allowing their inclusion in an HB framework. The numerical examples presented in Chapter 5 demonstrate the feasibility of the proposed method and the results obtained from this method were compared to theory and responses generated using OptiSPICE.

6.2 Future Work

The work performed as part of this thesis forms the basis for several interesting directions in the future. This section provides a brief description of these directions.

- **An optimized implementation:** the current implementation of proposed method is performed in MATLAB and is not fully optimized. Future work can be undertaken to optimize the proposed algorithm and implement it in an object-oriented programming language such as C++ or Objective-C.

- **Steady-state response of digital optoelectronic systems:** Harmonic Balance technique [26,27] is typically used for simulation of analog systems having smooth waveforms at the steady-state. Generally, for a digital system it is not

efficient to use HB due to the need of a large number of harmonics to capture the steady-state waveform. For a single-tone digital system typically Shooting Method (SM) is well suited; although, for a quasi-tone system which is the case of typical digital optical waveforms, SM becomes impractical since finding the global period of the waveform is a burden. In this situation, using a mixed frequency-time domain technique [26] might be usefull, in which SM is used for capturing the digital envelope while the sinusoidal optical carrier is solved in frequency-domain using HB. Future work can be performed to investigate the performance of mixed frequency-domain techniques for obtaining the steady-state response of digital optoelectronic systems.

- **Other optical components:** In the presented work, the simulation models for the laser diode, linear optical fiber, photodiode, and interference based devices, presented in Chapter 3, are studied to be used in the HB framework; however, still there are several optical components [1, 2, 23, 67] which likely require more investigations to be modeled in the HB framework. Examples of these optical devices are Mach-Zehnder modulators, Semiconductor Optical Amplifiers (SOAs), optical filters, and non-linear single-mode fibers.

Appendix A

Delay Element Model

Figure 26 shows the input and output of a delay element as used in optical fiber model. At steady-state an AP waveform can be expressed using truncated Fourier series as

$$E(t) = E_0 + E_1^c \cos(\lambda_1 t) + E_1^s \sin(\lambda_1 t) + ... + E_M^c \cos(\lambda_M t) + E_M^s \sin(\lambda_M t). \quad \text{(A.1)}$$

Applying the delay of τ_d to (A.1), the delayed waveform can be written as

$$E(t-\tau_d) = E_0 + E_1^c \cos(\lambda_1 t - \lambda_1 \tau_d) + E_1^s \sin(\lambda_1 t - \lambda_1 \tau_d) + \\ ... + E_M^c \cos(\lambda_M t - \lambda_M \tau_d) + E_M^s \sin(\lambda_M t - \lambda_M \tau_d). \quad \text{(A.2)}$$

In order to find the input/output Fourier coefficiants relation, using

$$\sin(X - Y) = \sin(X)\cos(Y) - \cos(X)\sin(Y), \quad \text{(A.3)}$$

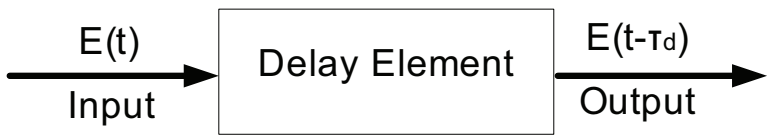

Figure 26: Delay element.

$$\cos(X - Y) = \cos(X)\cos(Y) + \sin(X)\sin(Y), \tag{A.4}$$

(A.2) can be written as

$$E(t-\tau_d) = E_0 + E_1^{'c}\cos(\lambda_1 t) + E_1^{'s}\sin(\lambda_i t) + ... + E_M^{'c}\cos(\lambda_M t) + E_M^{'s}\sin(\lambda_M t), \tag{A.5}$$

in which,

$$E_i^{'c} = E_i^c\cos(\lambda_i\tau_d) - E_i^s\sin(\lambda_i\tau_d), \tag{A.6}$$

$$E_i^{'s} = E_i^c\sin(\lambda_i\tau_d) + E_i^s\cos(\lambda_i\tau_d). \tag{A.7}$$

Above equations can be shown in a matrix form as

$$\begin{bmatrix} E_i^{'c} \\ E_i^{'s} \end{bmatrix} = \begin{bmatrix} \cos(\lambda_i\tau_d) & -\sin(\lambda_i\tau_d) \\ sin(\lambda_i\tau_d) & \cos(\lambda_i\tau_d) \end{bmatrix} \begin{bmatrix} E_i^c \\ E_i^s \end{bmatrix}. \tag{A.8}$$

Incorporating fiber attenuation, the input/ouput relation of a fiber is given by (4.31).

List of References

[1] J. Yao, "Microwave photonics," *J. Opt Soc.*, vol. 27, no. 3, February 2009.

[2] A. J. Seeds and K. J. Williams, "Microwave photonics," *J. Lightwave Technol.*, vol. 24, no. 12, pp. 4628–4641, December 2006.

[3] A. Seeds, F. Pozzi, C. Renaud, M. Fice, and L. Ponnampalam, "Microwave photonics: opportunities for photonic integration," in *14th European Conf. on Integrated Optics*.

[4] J. Capmany and D. Novak, "Microwave photonics combines two worlds," *Nature Photonic*, vol. 1, pp. 319–330, June 2007.

[5] I. Gasulla, J. Lloret, J. Sancho, S. Sales, and J. Capmany, "Recent breakthroughs in microwave photonics," *IEEE Photonics J.*, vol. 3, no. 2, pp. 311–315, April 2011.

[6] B. Jalali and S. Fathpour, "Silicon photonics," *J. Lightwave Technol.*, vol. 24, no. 12, pp. 4600–4615, December 2006.

[7] J. Capmany, I. Gasulla, and S. Sales, "Microwave photonics harnessing slow light," *Nature Photonics*, vol. 5, pp. 731–733, December 2011.

[8] S. Ristic, A. Bhardwaj, M. J. Rodwell, L. A. Coldren, and L. A. Johansson, "An optical phase-locked loop photonic integrated circuit," *J. Lighwave Technol.*, vol. 28, no. 4, pp. 526–538, February 2010.

[9] R. Nagarajan, C. Joyner, J. Schneider, R. P. Schneider, J. Bostak, T. Butrie, A. Dentai, V. Dominic, P. Evans, M. Kato, M. Kauffman, D. Lambert, S. Mathis, A. Mathur, R. Miles, M. Mitchell, M. Missey, S. Murthy, A. Nilsson, F. Peters, S. Pennypacker, J. Pleumeekers, R. Salvatore, R. Schlenker, R. Taylor, H. Tsai, M. V. Leeuwen, J. Webjorn, M. Ziari, D. Perkins, J. Singh, S. Grubb, M. Reffle, D. Mehuys, F. Kish, and D. Welch, "Large-scale photonic integrated circuits,"

IEEE Trans. Sel. Topics Quantum Electron., vol. 11, no. 1, p. 5065, February 2005.

[10] S. Levitan, T. Kurzweg, P. Marchand, M. Rempel, D. Chiarulli, J. Martinez, J. Bridgen, C. Fan, and F. McCormick, "Chatoyant: a computer-aided design tool for free-space optoelectronic systems," *Appl. Opt.*, vol. 37, no. 26, pp. 6078–6092, September 1998.

[11] M. Kahrs, S. P. Levitan, D. M. Chiarulli, T. P. Kurzweg, J. A. Martnez, J. Boles, A. J. Davare, E. Jackson, C. Windish, F. Kiamilev, A. Bhaduri, M. Taufik, X. Wang, A. S. Morris, J. Kruchowski, , and B. K. Gilbert, "System-level modeling and simulation of the 10G optoelectronic interconnect," *J. Lightwave Technol.*, vol. 21, no. 12, pp. 3244–3256, December 2003.

[12] P. Gurney and A. Lowery, "OPALS: new computer aided learning package for photonics," in *Proc. Multi-Media Engineering Education*, 1994, pp. 115–123.

[13] A. Lowery, "New dynamic semiconductor laser model based on the transmission-line modelling method," *Optoelectronics, IEE Proceedings*, vol. 134, no. 5, pp. 281–289, October 1987.

[14] B. Whitlock, J. Morikuni, E. Conforti, and S.-M. Kang, "Simulation and modeling: simulating optical interconnects," *IEEE Circuits and Devices Magazine*, vol. 11, no. 3, pp. 12–18, October 1995.

[15] A. Yang and S. Kang, "iSMILE: A novel circuit simulation program with emphasis on new device model development," in *26th Conf. on Design Automation*, 1989, pp. 630–633.

[16] M. A. Neifeld and W.-C. Chou, "SPICE-based optoelectronic system simulation," *Appl. Opt.*, vol. 37, no. 26, pp. 6093–6104, September 1998.

[17] A. Lowery, "Computer-aided photonics design," *IEEE Spectrum*, vol. 34, no. 4, pp. 26–31, April 1997.

[18] D. M. Byrne, "SPICE-based CAD modeling of high-speed data links," in *Conf. on Optical Fiber Communications*, 1992.

[19] M. Fashano and A. Strodtbeck, "Communication system simulation and analysis with SYSTID," *IEEE J. Selected Areas in Communications*, vol. 2, no. 1, pp. 8–29, January 1984.

[20] K. S. Shanmugan, "An update on software packages for simulation of communication systems," *IEEE J. Selected Areas in Communications*, vol. 6, no. 1, pp. 5–12, January 1988.

[21] C. L. Brun, E. Guillard, , and J. Citerne, "Communication systems interactive software (COMSIS): modeling of components and its application to the simulation of optical communication systems," *Appl. Opt.*, vol. 37, no. 26, September 1998.

[22] S. W. Lee, E. C. Choi, , and W. Y. Choi, "Optical interconnection system analysis using SPICE," in *Conf. on Lasers and Electro-Optics*, 1999, pp. 391–392.

[23] P. Gunupudi, T. Smy, J. Klein, , and Z. Jakubczyk, "Self-consistent simulation of opto-electronic circuits using a modified nodal analysis formulation," *IEEE Trans. Advanced Packaging*, vol. 33, no. 4, pp. 979–993, November 2010.

[24] C. Hoqq, A. Ruehli, , and P. Brennan, "The modified nodal approach to network analysis," *IEEE Trans. on Circuits and Systems*, vol. 22, pp. 504–509, June 1975.

[25] J. Vlach and K. Singhal, *Computer methods for circuit analysis and design.* New York: Van Nostrand Reinhold, 1983.

[26] K. S. Kenneth, J. K. White, and A. Sangiovanni-Vincentelli, *Steady-state methods for simulating analog and microwave circuits.* MA: Kluwer Academic, 1990.

[27] P. Rodrigues, *Computer-aided analysis of nonlinear microwave circuits.* Boston: Artech House, 1997.

[28] T. J. Aprille and T. N. Trick, "Steady-state analysis of nonlinear circuits with periodic inputs," *Proc. IEEE*, vol. 60, no. 1, pp. 108–114, January 1972.

[29] M. S. Nakhla and Jiri, "A piecewise harmonic balance technique for determination of periodic response of nonlinear systems," *IEEE Trans. Circuits and Systems*, vol. 7, no. 4, pp. 85–91, August 1976.

[30] D. Long, R. Melville, K. Ashby, and B. Horton, "Full-chip harmonic balance," in *Proc. IEEE Custom Integrated Circuits Conf.*, Santa Clara, CA, 1997, pp. 379–382.

[31] D. Feng, J. Phillips, K. Nabors, K. Kundert, and J. White, "Efficient computation of quasi-periodic circuit operating conditions via a mixed frequency/time approach," in *Proc. 36th Design Automation Conf.*, 1999, pp. 635–640.

[32] P. Feldmann and J. Roychowdhury, "Computation of circuit waveform envelopes using an efficient, matrix-decomposed harmonic balance algorithm," in *IEEE/ACM Int. Conf. on Computer-Aided Design*, San Jose, CA, USA, 1996, pp. 295 –300.

[33] V. Rizzoli, A. Neri, and F. Mastri, "A modulation-oriented piecewise harmonic-balance technique suitable for transient analysis and digitally modulated signals," in *Proc. 26th Microwave Conf.*, Czech Republic, 1996, p. 546550.

[34] H. Brachtendorf, G. Welsch, R. Laur, and A. Bunse-Gerstner, "Numerical steady state analysis of electronic circuits driven by multi-tone signals," *Electrical Engineering*, vol. 79, p. 103112, December 1996.

[35] J. Roychowdhury, "Efficient methods for simulating highly nonlinear multi-rate circuits," in *Proc. 34th Design Automation Conf.*, Czech Republic, 1997.

[36] S. Maas, *Nonlinear Microwave Circuits.* Norwood, MA: Artech House, 1988.

[37] S. Iezekiel, C. Snowden, and M. Howes, "Harmonic balance model of laser diode," *Electronics Lett.*, vol. 25, no. 8, pp. 529–530, April 1989.

[38] ——, "Nonlinear circuit analysis of harmonic and intermodulation distortions in laser diodes under microwave direct modulation," *IEEE Trans. Microwave Theory and Tech.*, vol. 38, no. 12, pp. 1906–1915, August 1990.

[39] T. Zhang, R. Hicks, and R. Tucker, "Computer-aided design and analysis of lightwave/microwave systems," in *IEEE Int. Microwave Symp. Dig., Albuquerque*, NM, 1999, pp. 841–844.

[40] E. Gad, "Simulation of RF integrated circuits," University of Ottawa, Ottawa, Course Notes, 2007.

[41] C. Bailey and J. Lindenlaub, "Further results concerning the effect of frequency-selective fading on differentially coherent matched filter receivers," *IEEE Trans. Communication Technol.*, vol. 16, no. 5, pp. 749–751, October 1968.

[42] "Guide to Harmonic Balance simulation in ADS," Agilent Technol., CA, U.S.A., Tech. Rep., September 2004.

[43] J. Bolstad and H. Keller, "A multigrid continuation method for elliptic problems with folds," *SIAM J. Sci. Statist. Comput.*, vol. 7, no. 4, pp. 1081–1104, August 1990.

[44] K. S. Kundert and A. Songiovanni-Vincentelli, "Sparse user's guide-a sparse linear equation solver," University of California, Berkeley, CA, Course Notes, 1988.

[45] K. S. Kenneth, G. B. Sorkin, and A. Sangiovanni-Vincentelli, "Applying harmonic balance to almost-periodic circuits," *IEEE Trans. Microwave Theory and Tech.*, vol. 36, no. 2, p. 366378, Februrary 1988.

[46] G. B. Sorkin, K. S. Kenneth, and A. Sangiovanni-Vincentelli, "An almost-periodic fourier transform for use with harmonic balance," in *IEEE MTT-S Int.*, Palo Alto, CA, USA, 1987, pp. 717–720.

[47] P. Rodrigues, "An orthogonal almost-periodic fourier transform for use in nonlinear circuit simulation," *IEEE Microwave and Guided Wave Lett.*, vol. 4, no. 3, pp. 74–76, March 1994.

[48] A. Usihda and L. Chua, "Frequency-domain analysis of nonlinear circuits driven by multi-tone signals," *IEEE Trans. Circuits and Systems*, vol. 31, no. 9, p. 766779, September 1984.

[49] L. Chua and A. Usihda, "Algorithms for computing almost periodic steady-state response of nonlinear systems to multiple input frequencies," *IEEE Trans. Circuits and Systems*, vol. 28, no. 10, p. 953971, October 1981.

[50] V. Rizzoli, C. Cecchetti, A. Lipparini, and F. Mastri, "General-purpose harmonic balance analysis of nonlinear microwave circuits under multitone excitation," *IEEE Trans. Microwave Theory and Tech.*, vol. 36, no. 12, pp. 1650–1660, December 1988.

[51] A. Usihda, L. Chua, and T. Sugawara, "A substitution algorithm for solving nonlinear circuits with multi-frequency components," *Int. J. Circuit Theory Applicat.*, vol. 15, no. 12, p. 327355, December 1987.

[52] P. L. Heron and M. B. Steer, "Jacobian calculation using the multidimensional fast Fourier transform in the harmonic balance analysis of nonlinear circuits," *IEEE Trans. Microwave Theory and Tech.*, vol. 38, no. 4, pp. 429–431, April 1990.

[53] D. Hente and R. Jansen, "Frequency domain continuation method for the analysis and stability investigation of nonlinear microwave circuits," *Microwaves, Antennas and Propagation, IEE Proceedings H*, vol. 133, no. 5, pp. 351–362, October 1986.

[54] M. Heimlich, T. Tinttunen, and V. Karanko, "The Advantages of Multi-Rate Harmonic Balance (MRHB)- Advanced, Multi-Tone Harmonic Balance Technology Pioneered by AWR," AWR Corporation, El Segundo, CA 90245, USA, White Paper.

[55] R. C. Melville, P. Feldmann, and J. Roychowdhury, "Efficient multi-tone distortion analysis of analog integrated circuits," in *Proc. IEEE Custom Integrated Circuits*, Santa Clara, CA, 1995.

[56] ——, "Efficient steady-state analysis based on matrix-free Krylov-Subspace methods," in *32nd Conf. on Design Automation*, Santa Clara, CA, 1995, pp. 480–484.

[57] R. Telichevesky, K. Kundert, I. Elfadel, and J. White, "Fast simulation algorithms for RF circuits," in *Conf. IEEE Custom Integrated Circuits*, Santa Clara, CA, 1996, pp. 437– 444.

[58] V. Rizzoli, F. Mastri, F. Sgallari, and G. Spaletta, "Harmonic Balance simulation of strongly nonlinear very large-size microwave circuits by inexact Newton methods," in *IEEE MTT-S Digest*, San Francisco, CA, USA, 1996, pp. 1357–1360.

[59] M. M. Gourary, S. G. Rusakov, S. L. Ulyanov, M. M. Zharov, K. K. Gullapalli, and B. J. Mulvaney, "Iterative solution of linear systems in Harmonic Balance analysis," in *IEEE MTT-S Digest*, San Francisco, CA, USA, 1997, pp. 1507–1510.

[60] J. Eker, J. Janneck, E. Lee, J. Liu, X. Liu, J. Ludvig, S. Neuendorffer, S. Sachs, and Y. Xiong, "Taming heterogeneity-the ptolemy approach," *Proc. IEEE*, vol. 91, no. 1, p. 27144, January 2003.

[61] T. Quarles, A. Newton, D. Pederson, and A. Sangiovanni-Vincentelli, "SPICE 3 version 3F5 users manual," University of California, Berkeley, CA, Course Notes.

[62] G. Agrawal, *Fiber-Optic Communication Systems.* New York: Wiley, 2003.

[63] C. DeCusatis, *Fiber Optic Data Communication.* New York: Elsevier, 2008.

[64] J. C. Cartledge and R. C. Srinivasan, "Extraction of DFB laser rate equation parameters for system simulation purposes," *J. Lightwave Technol.*, vol. 15, no. 4, pp. 852–860, March 1997.

[65] P. V. Mena, J. J. Morikuni, S. M. Kang, A. V. Harton, and K. W. Wyatt, "A simple rate-equation-based thermal VCSEL model," *J. Lightwave Technol.*, vol. 17, no. 5, pp. 865–872, May 1999.

[66] J. Campbell, B. Johnson, G. Qua, and W. Tsang, "Frequency response of Inp/InGaAsP/InGaAs avalanche photodiodes," *J. Lightwave Technol.*, vol. 7, no. 5, p. 778784, May 1989.

[67] R. Ramaswami, K. Sivarajan, and G. Sasaki, *Optical Networks, A Practical Perspective.* New York: Elsevier, 2009.

[68] P. Pepeljugoski, S. E. Golowich, A. J. Ritger, P. Kolesar, and A. Risteski, "Modeling and simulation of next-generation multimode fiber links," *J. Lightwave Technol.*, vol. 21, no. 5, pp. 1242–1255, May 2003.

[69] T. Smy, P. Gunupudi, S. McGarry, and W. N. Ye, "Circuit-level transient simulation of configurable ring resonators using physical models," *J. Opt. Soc.*, vol. 28, no. 6, June 2011.